NASA TN D-1657

TECHNICAL NOTE
D-1657

CHARGE-EXCHANGE EFFECTS ON THE ACCELERATOR IMPINGEMENT OF AN ELECTRON-BOMBARDMENT ION ROCKET

By William R. Kerslake

Lewis Research Center
Cleveland, Ohio

NATIONAL AERONAUTICS AND SPACE ADMINISTRATION
WASHINGTON

May 1963

NATIONAL AERONAUTICS AND SPACE ADMINISTRATION

TECHNICAL NOTE D-1657

CHARGE-EXCHANGE EFFECTS ON THE ACCELERATOR IMPINGEMENT OF AN ELECTRON-BOMBARDMENT ION ROCKET

By William R. Kerslake

SUMMARY

A systematic investigation of accelerator-grid-ion impingement was made with electron-bombardment ion rockets operated over a range of propellant utilization efficiencies from 0.11 to 0.95. Three ion rockets of 5, 10, and 20 centimeters in diameter were used to produce mercury-ion beams of 0.01 to 0.55 amperes at net accelerating potentials of 600 to 7000 volts. Trends of experimental impingement values were predicted by ion charge-exchange equations, particularly below propellant utilization efficiencies of 0.6. Discrepancies between experimental and predicted values were probably caused by direct impingement ions. Calculations were made to estimate the maximum lifetime of a molybdenum accelerator grid based upon the rocket operation parameters, charge-exchange equations, and the measured erosion rate of an endurance run. The experimental work was conducted in a 5-foot-diameter, 16-foot-long vacuum tank.

INTRODUCTION

An electron-bombardment ion rocket will always have some nonionized propellant flowing out through the accelerator grid. These neutral propellant molecules (or atoms) may undergo charge-exchange collisions with the ion beam, which is moving through the same region. The charge-exchange process produces high-velocity neutrals that will continue on away from the thrustor and also produces low-velocity ions, which will most probably be drawn to the accelerator grid. This current of ions will be read as impingement current, the same as directly impinging ions, and will also do sputtering damage to the accelerator grid.

The results of reference 1 show that a large part of the impingement current may be due to charge exchange. These results were reported for an ion thrustor running at a propellant utilization efficiency of 0.8 (ratio of ions out to neutral molecules in) and mounted in a bell jar connected to a vacuum tank. For the investigation reported herein the ion thrustor was moved directly into the vacuum tank where the surrounding neutral pressure would be lowered to a negligible amount. Tests were then run over a wide range of propellant utilization efficiencies to study the effect of neutral propellant density on the accelerator impingement and on the operation of the ion thrustor. Data were then

taken for 5-, 10-, and 20-centimeter-diameter ion thrustors; however, most of the tests were performed with the 10-centimeter-diameter thrustor.

Also included herein are lifetime estimates of an accelerator grid based on calculated impingement currents resulting from the charge-exchange process. The rate of erosion was determined by measurements made on an accelerator grid used in the 150-hour endurance run of reference 2.

APPARATUS AND PROCEDURE

The ion thrustors used in these experiments were mounted in a vacuum tank, 5 feet in diameter and 16 feet long. Figure 1 is a cutaway drawing of the vacuum tank showing the position of the ion thrustor, suppressor screen, cold baffles, and two of the tank ion gages. The tank was evacuated by three 32-inch-diameter oil-diffusion pumps with liquid-nitrogen cold traps to stop oil backstreaming. The suppressor screen prevented secondary electrons from traveling from the tank region back to the thrustor, which runs at a high positive potential.

The liquid-nitrogen-cooled surfaces contained an area of approximately 33 square meters, which with the diffusion pumps enabled the tank to be evacuated to 5×10^{-7} to 9×10^{-7} mm Hg. With the ion thrustor operating, the tank pressure was 1.3×10^{-6} to 7.6×10^{-6} mm Hg. The tank pressure was measured with hot-filament ion gages located on the walls of the tank and shielded from direct sight of the thrustor (see fig. 1). The tank ion gages generally read within 0.5×10^{-6} mm Hg of each other.

Figure 2 is a cutaway sketch of the 10-centimeter-diameter thrustor with the aperture of an ion gage positioned 7.6 centimeters downstream of the accelerator grid and 7.6 centimeters radially from the centerline of the beam. The ion source of the thrustor is identical to the source used throughout reference 1. The 5- and 20-centimeter-diameter sources were made geometrically similar to the 10-centimeter-diameter thrustor except for slight variations of the magnetic fields and differences of the screen-accelerator grids. The 5- and 20-centimeter sources were first reported in reference 3, and further details of construction may be found there.

Gaseous mercury propellant was supplied at a steady rate by a steam-heated boiler through one of a series of interchangeable calibrated orifices. The mercury vapor passed through a thin-walled 5-centimeter-diameter stainless-steel tube that separated the boiler from the ion source. This tube shown in figure 2 resisted the conduction of heat from the hot (about 500° K) ion source to the boiler.

The mercury vapor from the boiler impinged on the distributor, which provided a relatively uniform influx of vapor to the ion chamber. The ion chamber, about 10 centimeters long, was bounded by a cylindrical anode 10 centimeters in diameter. (Nominal thrustor size is the anode diameter.) The emitter, a hairpin-shaped filament of 0.5-millimeter-diameter tungsten wire, was positioned along the axis of the ion chamber. In the operation of the source, electrons from the filament were accelerated towards the anode, producing ionizing colli-

sions and filling the chamber with a plasma. The ion chamber potential difference (discharge voltage) was held constant at 50 volts. An axial magnetic field, decreasing in strength in the downstream direction, was used to confine the electrons. The magnetic field strength was held approximately constant while operating a particular source but varied from source to source as shown in table I.

The ion-accelerating structure, comprising a molybdenum screen and a molybdenum accelerator grid at the downstream end of the chamber, extracted ions from the plasma and accelerated them as a beam. Nonionized molecules could diffuse through the accelerator plate openings into the vacuum tank. Aluminum-oxide balls supported and positioned the accelerator grids. Details of the grid spacings are also found in table I.

Figure 3 is a schematic drawing of the electrical system showing the anode as the highest positive voltage and the net potential through which the ions are accelerated. The ground-return meter reads the ion-beam current. Also shown are the filament heating supply, ion-chamber potential difference (filament bias) supply, magnetic field current supply, and accelerator supply.

The thrustor was assembled with a measured quantity of propellant in the boiler. The accelerator-screen grid spacing was determined at five random locations. The thrustor was then mounted in the vacuum tank and the facility pumped down. When the desired background pressure level was reached, the boiler was heated by flowing steam through a throttling valve to the boiler. As the mercury pool approached operating temperature (3 to 5 min) the electrical supplies were turned on. When a sufficient density of mercury vapor built up in the ion chamber, the discharge started. The electrical parameters were then adjusted to give the desired performance level.

Accelerator impingement data were taken with the thrustor operating with a constant propellant input. The beam current was varied to give propellant utilization efficiency η_u from 0.11 to a maximum of 0.95. (Symbols are defined in appendix A.) The propellant utilization efficiency is defined as the ratio of the number of ions flowing out (beam current) to the number of neutral propellant atoms or molecules flowing into the thrustor. At a constant value of beam current, the specific impulse or velocity (velocity $\propto \sqrt{\text{voltage}}$) of the ion beam was varied from a low voltage determined by space-charge limited ion flow, to a high voltage determined by the electrical breakdown limit between the accelerating grids. The filament-emission current was adjusted to hold the beam current at the desired value. The accelerator voltage was always set at a sufficient negative value to stop backstreaming electrons from reaching inside the thrustor and causing damage or false beam-current meter readings.

RESULTS AND DISCUSSION

Typical Accelerator Performance

Most of the accelerator performance data were obtained at constant beam current J_B and constant ratio of net- to total-accelerating potential R of 0.8, where R is $V_I/(V_I + |V_A|)$, and $(V_A < 0)$. For the purpose of comparison, some

data were also taken at values of R of 0.6 and 0.4. An R of 0.8 was sufficient to stop electron backstreaming. A more complete description of the effect of various values of R on thrustor operation can be found in reference 1.

Figure 4 is a plot of typical accelerator impingement current J_A data as a function of net accelerating potential V_I for constant beam current and R values. The curves are characterized by a sharp rise in accelerator impingement, corresponding to a space-charge limitation, as some critical low net accelerating potential value was reached. At higher voltages, an almost level operating region was obtained to a net accelerating potential where electrical breakdown occurred. Impingement curves for other beam current and R values were similar to figure 4 and are not plotted, although the data are included in table II.

Propellant Utilization Efficiency

Figure 5 shows a comparison of the experimental accelerator impingement data with estimated charge-exchange values calculated by the method of appendix B. Data are presented for 5-, 10-, 20-centimeter-diameter thrustors in figures 5(a), (b), and (c), respectively, with R = 0.8. Figures 5(d) and (e) are plotted for different R values with the 10-centimeter source.

For all the data of figure 5, there is a general increase in the percent of impingement current as propellant utilization efficiency is decreased. The nonionized mercury must pass out of the thrustor through the accelerator grids and, hence, must be subjected to charge-exchange collisions. The variation of impingement current with propellant utilization efficiency is therefore interpreted as largely due to charge exchange.

The percent of a beam that undergoes charge exchange is approximately proportional to the product of three quantities, (1) the neutral density, (2) the distance of beam travel, and (3) the charge-exchange cross section. Details of the derivation of the theoretical equation and the values used therein are presented in appendix B. Basically, the neutral density is determined by the mercury input J_o and the propellant utilization efficiency, by assuming singly charged beam ions. The distance traveled by the beam is the sum of two parts; one, the distance between the screen and accelerator grid, and the other, the downstream beam-deceleration distance. While the grid spacing was constant, the calculated downstream deceleration distance varied with the operating conditions The collision cross section value was available in the literature for mercury ions through mercury neutrals.

Most of the experimental accelerator currents were higher than the calculated values. This difference was attributed to direct impingement on the accelerator grid. Direct impingement may result from the ion optics of the acceleration structure, misalinement of the accelerator grid due to machining tolerances and thermal expansion effects, and variable discharge characteristics of the ion chamber. The high direct inpingement of run 6 was probably caused by the closer spacing or smaller $l_{\text{¢}}/D$ value of the accelerator system. The case of operation at lower R or more accel-decel voltage, as in figure 5(d) and (e)

subjects the calculation to greater possible errors because of a longer beam decel region, and may account for the discrepancy of run 4 at R = 0.6 and 0.4.

A constant value of net accelerating potential was picked for each run to facilitate the comparison of data and the calculation of theoretical curves. The value picked was on the level portion of the curve of the accelerator-impingement current as a function of net accelerating potential for each constant beam current. The range of net accelerating potential was fixed between the space-charge limited current and electrical breakdown, and this range varied depending upon the beam current and grid spacing.

Operation of the ion thrustor in the vacuum tank instead of in a bell jar as for reference 1 resulted in a background neutral density of about 1 decade less (10^{-6} mm Hg scale instead of 10^{-5} mm Hg for the ionization gage readings). The lower tank neutral density combined with a probable lower charge-exchange cross section (lower by one order of magnitude or more (ref. 4)) for nonmercury neutrals reduces the error caused by charge-exchange impingement of the tank neutrals to a negligible amount.

The experimental values of accelerator-impingement current became higher at lower propellant utilization efficiency, and the increase probably was caused entirely by charge-exchange current. At values of propellant utilization efficiency higher than 0.7, charge-exchange impingement currents fell to lower values, and direct impingement may become equal to or greater than that from charge exchange. At the higher propellant utilization efficiencies any doubly ionized atoms would cause a sideways shift in the predicted curve. Although doubly ionized atoms have been neglected, they could be as much as 10 percent of the total beam. A 10-percent value of double ions would increase η_u by a factor of 1.1 in figure 5. As a result, the zero-percent impingement current would go through a propellant utilization efficiency of 1.1 instead of 1.0.

Ionization Gage Readings

Figure 6 is a plot of the readings of two standard hot-filament ionization gages taken while the ion thrustor was operating. The gage located on the tank wall, out of line of sight of the thrustor, read an equilibrium tank pressure. This tank gage read a minimum pressure with the thrustor discharge off and linearly increased as the ion-beam current increased. The total flow of mercury particles was constant throughout, but as the number of accelerated ions became greater, the tank pressure reading increased. This dependence of tank pressure on beam current and ion-beam energy is described in reference 5.

The gage located near the thrustor outlet was surrounded by its normal glass envelope, but the neck of the tube was cut back to the envelope to produce an aperture in the envelope. This aperture could directly sample the mercury molecules diffusing from the thrustor. With the ion-chamber discharge off ($\eta_u = 0$), all mercury flow from the thrustor consisted of neutral molecules, as a result, the gage read a maximum. The tank gage did not sense this neutral flow because the liquid nitrogen baffles cryopumped the mercury before it reached the tank gage location. As the ion-beam current was increased, the thrustor outlet gage

read less because the neutral flow was proportionately smaller with constant propellant input to the thrustor. If the propellant utilization efficiency were extrapolated to 100 percent, the readings of the two gages would be the same because neutral mercury would not be leaving the thrustor and thus would not cause the thrustor outlet gage to read higher. Both gages would read the same equilibrium tank pressure produced by the random energetic particles of the tank. (Typical beam ions probably make three to five wall collisions before condensing.)

The level of the thrustor outlet gage reading was very sensitive to location and thrustor operating conditions. If it was too close to the thrustor, the gage read over scale because of excess mercury. If it was too far from the thrustor, the increase of pressure due to the mercury neutrals was so small it was masked by normal tank pressure fluctuations. The gage would also read too high if the thrustor operation produced a divergent ion beam. Ions would then enter the gage directly at a higher velocity and rate than the neutrals and produce a false high reading.

If the neutral efflux is assumed to follow the cosine distribution originating from the accelerator plane, the ion gage reading can be predicted. Such a calculation was made for the 100-percent neutral flow case, and the result agreed with the observed values of the ion gage to within 20 percent. A gage sensitivity of three times the indicated value was used for mercury gas.

Space-Charge Limited Current

The ratio of measured current to current determined by Child's law is plotted as a function of propellant utilization efficiency in figure 7. Current determined by Child's law was calculated from the following equation:

$$J_B = 0.386 \times 10^{-8} \frac{A_A (\Delta V)^{3/2}}{r_{\ell}^2} \qquad (1)$$

where the charge-to-mass ratio for singly ionized mercury was used. The knee of a typical curve of accelerator impingement as a function of net accelerating potential (as in fig. 4) was used to determine the total accelerating voltage between grids ΔV. Since neutrals are uncharged, the space-charge limited current would not be expected to vary with propellant utilization efficiency. The experimental data, however, show a decrease in space-charge limited current as propellant utilization efficiency was reduced. This reduction in the ability to pass current indicates that the beam area is shrinking as the propellant utilization efficiency is lowered. Presumably, the ion chamber discharge is not required to produce as many ions, and the first ionizing collisions near the axis or filament can supply sufficient ions for the beam. As the neutral input flow is spread uniformly across the ion chamber by the distributor, the discharge for high utilizations must extend almost to the anode diameter to reach a sufficient number of atoms; thus a larger effective beam area results.

Accelerator Grid Erosion

A detailed analysis was made of the molybdenum accelerator grid used in the 150-hour endurance run of reference 2. Enlargements of photographs taken after the run were used to measure individual hole wear in the accelerator grid. The grid when new was 0.127 centimeter thick with 0.476-centimeter-diameter holes on 0.635-centimeter triangle centers. The endurance run was made with a 10-centimeter-diameter thrustor at a beam current of 0.2 ampere with a net accelerating potential of 2500 volts and an accelerator potential of -2000 volts. The average accelerator impingement current during the run was 4×10^{-3} amperes.

Photographs before and after the endurance run are shown in figure 8. The downstream face showed more pronounced erosion effects. There was little change in the thickness of the grid or in the diameter of the hole of the upstream face. The eroded downstream face hole diameter D' was greatly enlarged. Figure 9 shows the variation in D' from maximum wear at the thrustor axis to negligible wear at the outer radius. Hole measurements were made from enlarged photographs of those shown in figure 8.

The erosion pattern is in good agreement with the beam profile measurements taken in reference 1. If the erosion of material is a uniform taper from D to D' for each hole, a calculated weight loss can be made by using the wear profile of figure 9. (A correction in D was made based on radial hole measurements made on the upstream face.) The calculated weight loss agreed within 5 percent of the 2.3 gram measured weight loss. The spread in the measured hole diameters at the outer radial dimension is probably the result of normal drilling tolerance or optical distortion of the photograph near the edges.

Based on a linearly extrapolated rate of erosion of the web thickness between holes, a conservative lifetime of 820 hours is predicted to erode the downstream web thickness to zero. The grid may not fail at this condition for there is still a triangular-shaped web section remaining. The total impingement tolerable for this particular accelerator grid is then 4×10^{-3} ampere impingement current times 820 hours or 3.28 ampere-hours. The value of 3.28 ampere-hours of erosion will be used as a basis for future calculations of a 10-centimeter-diameter accelerator grid lifetime. The assumption is made that the erosion is proportional to the total impingement and not the rate of impingement.

Calculated Grid Lifetimes

The principal wear of a properly designed accelerator can be attributed to charge-exchange ions. As shown in appendix B, such an ion current J_A can be calculated as a function of thrustor operating conditions. Additionally, the total allowable impingement (3.28 amp-hr per 10-cm diam. beam) has been determined from extrapolated erosion measurements. Consequently, the accelerator lifetime of a 10-centimeter-diameter thrustor can be estimated by using this experimental wear rate and a calculated value of impingement current, J_A, from charge-exchange equations. The following equation can therefore be used:

$$t = \frac{3.28 \text{ amp-hr}}{J_A, \text{ amp}} \tag{2}$$

where J_A is determined from equation (B16). This lifetime will be the maximum to be expected, and any direct impingement will shorten the lifetime.

The result of such a calculation is shown in figure 10. Lifetimes may be predicted as a function of propellant utilization efficiency and beam current for the given values of V_I, R, and $l_{\text{¢}}$. The trends of figure 10 predict that an ion thrustor operated at a high propellant utilization efficiency and a low beam current or current density will obtain the longest accelerator-grid lifetime.

The calculated effect of a different net acceleration voltage V_I is to give an approximately 10-percent longer lifetime for 2000 volts and a 10-percent shorter lifetime for 4000 volts as compared to the normal lifetime for V_I = 3000 volts. Also, the effect of a different net- to total-acceleration voltage ratio R is shown in the following table:

R	Approximate relative lifetime
1.0	2
.8	1
.6	.5

For a lifetime of about 1 year and $\eta_u = 0.8$, the 10-centimeter-diameter thrustor used in the calculations should be operated at a beam current of about 0.15 ampere.

Another calculation was made to estimate the maximum lifetime for an ideal thrustor. For this purpose the following assumptions were made:

(1) Uniform radial wear of the accelerator grid (uniform beam profile). The lifetime impingement was assumed three times that of the endurance run because the wear is spread uniformly over the entire grid area (9.8 amp-hr per 10-cm diam. thrustor).

(2) No deceleration region to add additional charge-exchange current (R = 1.0).

The lifetime was calculated from

$$t = \frac{9.8 \text{ amp-hr}}{J_A} \tag{3}$$

where J_A is obtained from equation (B16), with $J_o = J_B/\eta_u$ and $f(R) = 0$.

Equation (B16) then becomes

$$J_A = 4.74 \frac{(1 - \eta_u)}{\eta_u} J_B^2 \frac{l\ell}{A_A} \tag{4}$$

Substituting J_A into equation (3) yields

$$t = \frac{9.8}{4.74 \frac{(1 - \eta_u)}{\eta_u} J_B^2 \frac{l\ell}{A_A}} \tag{5}$$

Using $j_B = (J_B/A_o) \times 10^4$ amperes per square meter and $A_A = 0.51\ A_o$ (typical grid flow-area fraction) results in

$$t l \ell j_B^2 = 1.35 \times 10^6 \left(\frac{\eta_u}{1 - \eta_u} \right) \tag{6}$$

This equation is valid for any size thrustor provided that the lifetime wear rate is 9.8 ampere-hours per 10-centimeter-diameter thrustor or 0.125 ampere-hour per square centimeter.

By using these assumptions, a maximum lifetime is predicted that cannot be exceeded, because the charge-exchange between grids cannot be avoided. Again, low beam-current density and high propellant utilization efficiencies lead to long accelerator grid lifetimes. For a 10-centimeter-diameter thrustor with the same operating conditions as used in figure 10, equation (6) indicates that a lifetime of a year could be obtained with a beam current of 0.31 ampere, or about twice that of the nonideal thrustor.

Sputtering Rate

The sputtering rate in grams per ampere-hour from three different references (refs. 4, 6, and 7) is plotted in figure 11 as a function of ion energy. The single data point was from the 150-hour endurance run of reference 2. The case of sputtering by charge-exchange ions is confused by two items. First, the exact energy of the charge-exchange ion is unknown because it depends on voltage level or position at which it was formed. Second, the angle of incidence is also unknown because it depends on the position of formation and the local electric field gradient. In general, the angle of incidence will be greater than zero and cause a higher sputtering rate; also, the charge-exchange ion will possess less energy than a direct impingement ion and hence, have a lower sputtering rate. These two factors may be balancing or they may weigh the sputtering rate either way. In the case of the endurance run, the actual sputtering rate was less than the predicted literature values for 2000 volts. A reasonable explanation is that most of the impingement was from charge-exchange ions at an average energy closer to 1000 volts. A modifying effect, neglected to this point, is secondary electrons that are ejected when ions strike the accelerator grid. This electron current is thought to be one-tenth or less of the impinging ion current in the

energy range up to several thousand electron volts. If these secondary electrons were produced, the measured sputtering value would be uncertain by 10 percent.

Electrical Breakdown of Thrustor

Figure 12 presents in graphical form the electrical breakdown data that is also included in table II. Breakdown values are reported with the ion thrustor operating. Breakdowns were more dependent on ΔV, the total voltage difference between the grids, rather than the individual voltage of either grid.

CONCLUDING REMARKS

The accelerator grid ion impingement was shown to consist mostly of charge-exchange ions at the lower propellant utilization efficiencies. If an ion thrustor could be operated near a propellant utilization efficiency of 1.0, the charge-exchange ions would approach zero because all the neutral molecules have been used to form beam ions. Due to practical considerations, an ion thrustor will always be operated at propellant utilizations below 1.0. Therefore, even though the accelerator system may be well focused, so that direct impingement is negligible, some erosion will still result from the charge-exchange ions. Once the operational level of propellant utilization efficiency has been determined, maximum accelerator-grid lifetime will be dictated by the unavoidable charge-exchange ions. For a 10-centimeter-diameter thrustor, a calculated 1-year lifetime could be obtained with a beam current of 0.15 ampere and a propellant utilization efficiency of 0.8. For the same size thrustor, but one having a uniform beam profile and no deceleration region, a calculated 1-year lifetime could be obtained with a beam current of 0.31 ampere and a propellant utilization efficiency of 0.8.

Lewis Research Center
National Aeronautics and Space Administration
Cleveland, Ohio, November 27, 1962

APPENDIX A

SYMBOLS

A_A	open area of accelerator or screen grid, sq cm
A_I	flow area of ions, sq cm
A_o	nominal thrustor area, sq cm
B	magnetic field strength at screen, gauss
D	new accelerator hole diameter, cm
D'	original accelerator hole diameter, cm
J_A	accelerator impingement current, amp
J_B	beam current, amp
J_E	filament emission current, amp
J_I	anode current, amp
J_M	magnetic field current, amp
J_o	inlet flow rate, amp
j_B	beam current density, $(J_B/A_o)\times 10^4$, amp/sq m
l	acceleration or deceleration distance, cm
$l_{\text{¢}}$	distance between grids, center of thickness, cm
m	molecular weight, amu
N	numbers of ions passing through uncharge-exchanged
N_I	total number of ions in beam
n_o	neutral mercury molecule density, molecules/cu cm
n_p	number density in a plane opening, molecules/cu cm
n_r	number density in a reservoir, molecules/cu cm
q	charge of an electron, coulomb
R	ratio of net- to total-acceleration voltage, $V_I/(V_I + \lvert V_A \rvert)$

r_p arrival rate at a plane, molecules/(sec)(sq cm)

T temperature, ^{o}K

t accelerator lifetime, hr

ΔV total acceleration voltage, $(V_I + |V_A|)$, v

V_A accelerator voltage, v

ΔV_F filament heater voltage, v

V_I anode total voltage and net ion acceleration voltage, v

ΔV_I anode-cathode discharge voltage, v

v velocity, cm/sec

$\bar{v}$ most probable velocity (thermal), 12,895 $\sqrt{T/m}$, cm/sec

x distance that ions travel for charge exchange, cm

β $\frac{4\epsilon_o}{9}\sqrt{2q/m} = 3.86\times10^{-9}$ mks units for Hg^{+1} ions

ϵ_o permittivity of free space, 8.85×10^{-12} coulomb^2/newton-meter^2

η_u propellant utilization efficiency, J_B/J_o

σ charge-exchange cross section, 6×10^{-15} sq cm

APPENDIX B

CALCULATION OF CHARGE-EXCHANGE CURRENT

The basic charge-exchange equation is

$$\frac{N}{N_I} = e^{-\sigma n_o x} \tag{B1}$$

and the fraction of ions losing their charge is

$$\frac{N_I - N}{N_I} = 1 - e^{-\sigma n_o x} \tag{B2}$$

In terms of currents, charge-exchange ions go to the accelerator grid as impingement current, J_A. Therefore,

$$\frac{N_I - N}{N_I} = \frac{J_A}{J_B} \tag{B3}$$

For small values of J_A/J_B (less than 0.05) the following approximation is valid:

$$1 - e^{-\sigma n_o x} = \sigma n_o x = \frac{J_A}{J_B} \tag{B4}$$

Cross Section

The value of 6×10^{-15} square centimeter for σ was obtained from reference 9 after extrapolating to an energy of 3000 volts. The value chosen was a compromise between a linear extrapolation of $\sqrt{\sigma}$ as a function of the logarithm of the square root of the ion energy and a smooth extrapolation of the trend of the data. A constant value of σ was used throughout this report because the trend of σ with voltage becomes flat for high voltages. The change in value of σ over the range of 2000 to 4000 volts is probably only several percent, while the error in extrapolating might be ±15 percent.

Arrival Rate and Number Density

The basis of determining n_o was the known flow rate of neutrals passing through the grid and the geometry of the grid. The approach used was to calculate n_o from arrival-rate equations for a plane and then modify n_o for the conductance effect of the grid holes. The differential equation for velocities in one direction is

$$\frac{dn}{n_r} = \frac{e^{-(v/\bar{v})^2}}{\sqrt{\pi}\ \bar{v}}\ dv \tag{B5}$$

where dn/n_r represents the fraction of particles in the velocity interval dv. The arrival rate at an opening r_p is the rate of particle arrival per unit area measured in the plane of the opening. The arrival rate of the fraction dn/n_r in the velocity interval dv is the product of the fraction and the approach velocity.

$$\frac{dr_p}{n_r} = v\ \frac{dn}{n_r}$$

Substituting equation (B5) results in

$$\frac{dr_p}{n_r} = \frac{e^{-(v/\bar{v})^2}}{\sqrt{\pi}\ \bar{v}}\ v\ dv \tag{B6}$$

Integrating v from 0 to $+\infty$ yields

$$\frac{r_p}{n_r} = \frac{\bar{v}}{2\sqrt{\pi}} \tag{B7}$$

Negative velocities are not considered because the particle density on the downstream side of the opening is assumed to be negligible.

The number density in the plane of the opening can be obtained by the following equation:

$$\frac{dn_p}{n_r} = \frac{e^{-(v/\bar{v})^2}}{\sqrt{\pi}\ \bar{v}}\ dv \tag{B8}$$

Integrating v from 0 to $+\infty$ yields:

$$\frac{n_p}{n_r} = \frac{1}{2} \tag{B9}$$

Combining equations (B7) and (B9) with $\bar{v} = 12{,}895\sqrt{T/m}$ and solving for n_p produces

$$n_p = \frac{r_p \sqrt{\pi m / T}}{12{,}895} \tag{B10}$$

The arrival rate r_p in terms of thrustor parameters is

$$r_p = 6.24\times10^{+18}\,\frac{(1-\eta_u)}{A_o}\,J_o \qquad \text{(B11)}$$

Substituting equation (B11) into equation (B10), using $m = 200.6$ for mercury, and assuming mercury atoms have $T = 530^{\circ}$ K (thrustor anode wall temperature) yields

$$n_p = n_o = 5.27\times10^{14}\,\frac{(1-\eta_u)}{A_o}\,J_o \qquad \text{(B12)}$$

Charge-Exchange Distance

Two parts of $\sigma n_o x$ have now been determined. The remaining factor, the charge-exchange distance, x, consists of two parts: (1) the distance between the screen and accelerator grids $l_{\text{¢}}$ and (2) a beam decelerating distance downstream of the thrustor. In this decelerating distance, charge-exchange ions will return to the accelerator grid. The distance $l_{\text{¢}}$ was chosen (from ref. 1) because this was the most accurate distance to use when computing ion flow characteristics. The deceleration distance was calculated from equation (45) of reference 10. This equation is

$$\frac{J_B}{A_I}\,\frac{l^2 R^{3/2}}{\beta V^{3/2}} = 1 + 3R^{1/2} - 4R^{3/2} \qquad \text{(B13)}$$

or

$$l^2 = \frac{\beta V_I^{3/2} A_I}{J_B}\left[\frac{1}{R^{3/2}} + \frac{3}{R} - 4\right] \qquad \text{(B14)}$$

where

$$R = \frac{V_I}{V_I + |V_A|}$$

Charge-Exchange Fraction

Substituting $J_B = \eta_u J_o$, $f(R) = (1/R^{3/2}) + (3/R) - 4$, and $x = l_{\text{¢}} + l$ into equation (B4) results in the following equation:

$$\frac{J_A}{J_B} = \underbrace{6\times10^{-15}}_{\sigma} \times \underbrace{5.27\times10^{14}\,\frac{(1-\eta_u)J_o}{A_o}}_{n_o} \underbrace{\left[l_{\text{¢}} + \sqrt{\frac{\beta V_I^{3/2} A_I}{\eta_u J_o}\,f(R)}\right]}_{x} \qquad \text{(B15)}$$

The value of n_o in equation (B12) is correct for the number density in the exit plane of the accelerator system. Due to conductance losses through the accelerator system, though, the mean density over the distance $l_{\text{¢}}$ is actually greater than n_o. In order to correct the neutral number density for flow losses it was assumed that free molecular flow would occur between the screen and accelerator holes as if there were a tube connecting them together. The length-to-diameter ratio of this tube would be about 1.0, and hence the entrance pressure or density would be twice that of the exit density. The tube exit is the plane of the accelerator hole, and it was this plane for which n_o was earlier calculated and used in equation (B15). The tube entrance number density would be $2n_o$ and the average number density over the length of the tube would be $1.5n_o$. Therefore for the portion of charge-exchange length, $l_{\text{¢}}$, in equation (B15), an average number density, $1.5n_o$, was used. With this factor of 1.5 and by combining terms (by using $A_A = A_I = 0.51\ A_o$, typical grid flow-area fraction, for the distance $l_{\text{¢}}$), equation (B15) becomes:

$$\frac{J_A}{J_B} = 3.16(1 - \eta_u)J_o \left[1.5\ \frac{l_{\text{¢}}}{A_A} + \sqrt{\frac{\beta V_I^{3/2} A_I}{A_o^2 \eta_u J_o}}\ f(R) \right] \tag{B16}$$

The ratio J_A/J_B was plotted in figure 5.

The flow area of the ions A_I was modified because of the shrinking of the beam from the full thrustor cross section, particularly at low propellant utilization efficiencies. The following table presents the values of A_I used in computing the theoretical curves in figure 5:

Nominal thrustor diameter, cm	Effective diameter for ion flow, cm	Effective flow area of ions, A_I, cm^2
5	5	19.6
10	5	19.6
20	10	78.4

The values used in the above table were based on general evidence of beam profiles, wear patterns on the accelerator grid, and visual observation of the discharge. The effective A_I value was an assumed mean value for the range of propellant utilization efficiencies covered. The following table lists for convenience the f(R) values used:

R	f(R)	R	f(R)
1.0	0	0.6	3.14
.8	1.14	.4	7.44

In summary, three quantities, σ, n_o, and x must be determined to calculate the charge-exchange current. The value of σ was obtained by extrapolating ($\pm$15 percent error) known literature values to the higher energies at which the present experimental data were taken. The value of n_o depended upon a neutral gas temperature assumption and molecular flow conductance calculation and might be in error by 50 percent. The value of x was based on a deceleration equation that was not experimentally proven or disproven and could also be in error by 50 percent. (As the deceleration distance depends upon current density, it could be shorter near the beam center and longer at the beam edges.) Consequently, although the most reasonable assumptions and physical parameters available were used, the resulting calculation of charge-exchange impingement current can only be regarded as accurate to a factor of two. There is no doubt, however, that the trends predicted by equation (B16) are correct.

Although charge-exchange current calculations may be in error, actual accelerator lifetimes depend only on impingement current and a rate of wear. Hence, where measurements of these two quantities are available, lifetimes can be closely estimated. Such measurements are included for one rate of wear from a 150-hour test and many determinations (for a short period of time) of impingement current as a function of ion thrustor parameters.

REFERENCES

1. Kerslake, William R.: Accelerator Grid Tests on an Electron-Bombardment Ion Rocket. NASA TN D-1168, 1962.

2. Reader, Paul D.: Investigation of a 10-Centimeter-Diameter Electron-Bombardment Ion Rocket. NASA TN D-1163, 1962.

3. Reader, Paul D.: Scale Effects on Ion Rocket Performance. ARS Jour. vol. 32, no. 5, May 1962, pp. 711-714.

4. Massey, H. S. W., and Burhop, E. H. S.: Electronic and Ionic Impact Phenomena. Clarendon Press (Oxford), 1956, pp. 448; 513; 514; 584.

5. Mickelsen, W. R., and Childs, J. H.: Theoretical Analysis of Ultrahigh Vacuum Condensers. Rev. Sci. Instr., vol. 29, no. 10, Oct. 1958, pp. 871-873.

6. Magnuson, G. D.: Sputtering Mechanisms Under Ion Propulsion Conditions. Fourth Quarterly Prog. Rep., Feb. 5 to May 5, 1962, General Dynamics Corp., May 10, 1962.

7. Wehner, G. K., and Rosenberg, D.: Mercury Ion Beam Sputtering of Metals at Energies of 4 to 15 kev. Jour. Appl. Phys., vol. 32, no. 5, May 1961, pp. 887-890.

8. Reader, Paul D., and Finke, Robert C.: An Electron-Bombardment Ion Rocket Operated with Alternating-Current Supplies. NASA TN D-1457, 1962.

9. Engel, Alfred: Ionized Gases. Clarendon Press (Oxford), 1955, p. 112.

10. Kaufman, Harold R.: One-Dimensional Analysis of Ion Rockets. NASA TN D-261, 1960.

TABLE I. - THRUSTOR DIMENSIONS, OPERATING CONDITIONS, AND CONSTANTS FOR EACH RUN

Run	Thrustor diameter, cm	Inlet flow, J_o, amp	Magnetic field strength at screen, B, gauss	Anode length, cm	Screen-accelerator grids				
					Original accelerator hole diameter, D, cm	Triangular hole spacing, cm	Grid thickness, cm	Grid spacing, l_{ℓ}, cm	l_{ℓ}/D
1	5	0.078	68	3.8	0.238	0.317	0.076	0.216	0.907
2	5	.164	68	3.8	.238	.317	.076	.216	.907
3	10	.080	44	7.5	.476	.635	.127	.447	.942
4	10	.165	41	7.5	.476	.635	.127	.444	.936
5	10	.327	44	7.5	.476	.635	.127	.439	.926
6	10	0.445	44	7.5	0.476	0.635	0.127	0.287	0.606
7	20	.175	18	14.3	.476	.635	.127	.350	.738
8	20	.465	12	14.3	.476	.635	.127	.350	.738
9	20	.970	12	14.3	.476	.635	.127	.350	.738

TABLE II. - INDIVIDUAL DATA POINTS

[Anode-cathode discharge voltage, -50 v; see table I for magnetic field strength and inlet flow.]

(a) Run 1

Anode total voltage and net ion acceleration voltage, V_I, v	Acceleration voltage, V_A, v	Beam current J_B, amp	Acceleration impingement current, J_A, amp	Anode current, J_I, amp	Filament emission current, J_E, amp	Propellant utilization efficiency, η_u	Tank pressure, mm Hg	Net- to total-acceleration voltage ratio, R
1500	-375	0.016	0.26×10^{-3}	0.25	0.20	0.20	--------	0.8
2000	-500	.016	.25	.21	.15	.20	--------	↓
3000	-750	.016	.27	.19	.13	.20	2.8×10^{-6}	
1500	-375	.031	.94	.68	.51	.40	--------	
2000	-500	.031	.38	.52	.42	.40	--------	
3000	-750	0.031	0.40×10^{-3}	0.42	0.31	0.40	--------	0.8
4000	-1000	.031	.40	.35	.28	.40	3.3×10^{-6}	↓
1600	-400	.047	4.55	1.22	1.05	.60	--------	
2000	-500	.047	.53	1.10	.91	.60	--------	
2500	-625	.047	.40	.90	.70	.60	--------	
3000	-750	0.047	0.40×10^{-3}	0.83	0.69	0.60	--------	0.8
4000	-1000	.047	.42	.72	.55	.60	3.9×10^{-6}	↓
1900	-475	.062	4.50	1.74	1.60	.80	--------	
2000	-500	.062	2.03	1.62	1.58	.80	--------	
2250	-560	.062	.80	1.55	1.52	.80	--------	
2500	-625	0.062	0.44×10^{-3}	1.50	1.48	0.80	--------	0.8
3000	-750	↓	.41	1.30	1.23	↓	--------	.8
4000	-1000		.40	1.15	1.03		3.9×10^{-6}	.8
4500	-1125		.44	1.00	.83		--------	.8
1600	-800		2.00	1.56	1.48		--------	.6
1650	-1100	0.062	0.80×10^{-3}	1.48	1.41	0.80	--------	0.6
1800	-1200	↓	.53	1.38	1.30	↓	--------	↓
2400	-1600		.53	1.20	1.09		--------	
3000	-2000		.56	1.01	.89		--------	
3600	-2400		.62	.90	.75		3.7×10^{-6}	
2500	-625	0.069	0.50×10^{-3}	1.75	1.89	0.89	--------	0.8
3000	-750	.070	.45	1.80	2.00	.90	--------	↓
3500	-875	.071	.42	1.81	2.08	.91	--------	
4000	-1000	.074	.45	1.85	2.10	.95	3.7×10^{-6}	
[a]4500	[a]-1125	[a].074	(a)	(a)	(a)	[a].95	(a)	[a].8

[a]Electrical breakdown.

TABLE II. - Continued. INDIVIDUAL DATA POINTS

[Anode-cathode discharge voltage, -50 v; see table I for magnetic field strength and inlet flow.]

(b) Run 2

Anode total voltage and net ion acceleration voltage, V_I, v	Acceleration voltage, V_A, v	Beam current, J_B, amp	Acceleration impingement current, J_A, amp	Anode current, J_I, amp	Filament emission current, J_E, amp	Propellant utilization efficiency, η_u	Tank pressure, mm Hg	Net- to total-acceleration voltage ratio, R
1400	-350	0.032	3.90×10^{-3}	0.62	0.50	0.20	--------	0.8
1600	-400	↓	1.57	.60	.50	↓	3.4×10^{-6}	↓
2000	-500		1.08	.50	.40		3.3	
3000	-750		1.08	.38	.30		--------	
4000	-1000		1.10	.30	.22		--------	
4500	-1125	0.032	1.11×10^{-3}	0.30	0.21	0.20	--------	0.8
[a]5000	[a]-1250	[a].032	(a)	(a)	(a)	[a].20	(a)	[a].8
2500	-625	.066	2.60	1.25	1.01	.40	--------	.8
2700	-675	.066	1.76	1.18	.95	.40	--------	.8
3000	-750	.066	1.62	1.01	.81	.40	3.5×10^{-6}	.8
4000	-1000	0.066	1.65×10^{-3}	0.89	0.70	0.20	--------	0.8
[a]5000	[a]-1250	[a].066	[a]1.74	[a].79	[a].61	[a].20	(a)	[a].8
3000	-750	.099	3.24	1.95	1.63	.60	3.7×10^{-6}	.8
3200	-800	.095	1.93	1.71	1.40	.58	--------	.8
3500	-875	.097	1.78	1.68	1.38	.59	--------	.8
4000	-1000	0.095	1.84×10^{-3}	1.53	1.25	0.58	--------	0.8
5000	-1250	.097	1.85	1.47	1.18	.59	3.8×10^{-6}	.8
2100	-1400	.095	5.96	1.91	1.60	.58	--------	.6
2400	-1600	.097	2.52	1.88	1.55	.59	--------	.6
3000	-2000	.097	2.31	1.72	1.41	.59	--------	.6
3600	-2400	0.098	2.45×10^{-3}	1.59	1.30	0.60	--------	0.6
3300	-825	.127	4.98	2.58	2.18	.78	--------	.8
3500	-875	.127	2.92	2.50	2.08	.78	--------	.8
4000	-1000	.127	2.09	2.40	1.98	.78	3.8×10^{-6}	.8
[a]4500	[a]-1125	[a].129	[a]2.16	[a]2.30	[a]1.91	[a].79	(a)	[a].8
3500	-875	0.150	7.80×10^{-3}	3.20	2.72	0.92	--------	0.8
3800	-950	.152	3.46	3.28	2.75	.93	--------	.8
4000	-1000	.154	2.79	3.20	2.70	.94	--------	.8
[a]4400	[a]-1100	[a].151	[a]2.81	[a]3.00	[a]2.50	[a].92	(a)	[a].8

[a]Electrical breakdown.

TABLE II. - Continued. - INDIVIDUAL DATA POINTS

[Anode-cathode discharge voltage, -50 v; see table I for magnetic field strength and inlet flow.]

(c) Run 3

Anode total voltage and net ion acceleration voltage, V_I, v	Acceleration voltage, V_A, v	Beam current, J_B, amp	Acceleration impingement current, J_A, amp	Anode current, J_I, amp	Filament emission current, J_E, amp	Propellant utilization efficiency, η_u	Tank pressure, mm Hg	Net- to total-acceleration voltage ratio, R
1200	-300	0.030	0.67×10^{-3}	0.60	0.55	0.38	--------	0.8
1300	-325	↓	.11	.60	.65	↓	--------	↓
1400	-350		.09	.50	.55		--------	
1600	-400		.09	.50	.55		--------	
2000	-500		.09	.45	.40		--------	
3000	-750	0.030	0.10×10^{-3}	0.40	0.35	0.38	--------	0.8
4000	-1000	↓	.11	.35	.35	↓	--------	↓
5000	-1250		.12	.35	.35		2.8×10^{-6}	
6000	-1500		.12	.30	.25		--------	
7000	-1750		.14	.25	.25		--------	
1400	-350	0.050	5.72×10^{-3}	1.80	----	0.63	--------	0.8
1600	-400	↓	1.41	1.80	----	↓	--------	↓
1800	-450		.21	----	----		--------	
1900	-475		.16	1.80	2.35		--------	
2000	-500		.11	1.55	----		--------	
3000	-750	0.050	0.13×10^{-3}	0.85	0.95	0.63	2.2×10^{-6}	0.8
4000	-1000	↓	.14	.80	----	↓	--------	↓
5000	-1250		.11	1.00	1.20		--------	
6000	-1500		.13	----	----		--------	
[a]7000	[a]-1750	[a].050	[a].17	(a)	(a)	[a].63	(a)	[a].8
1800	-450	0.060	2.79×10^{-3}	3.10	4.00	0.75	4.2×10^{-6}	0.8
2000	-500	↓	.93	1.90	2.40	↓	4.2	↓
2200	-550		.40	2.30	3.00		4.2	
2400	-600		.15	2.10	2.80		4.2	
3000	-750		.14	.99	1.00		4.3	
4000	-1000	0.060	0.15×10^{-3}	1.15	1.30	0.75	5.0×10^{-6}	0.8
5000	-1250	↓	.16	1.25	1.45	↓	5.0	.8
1500	-1000		.68	2.30	3.00		4.1	.6
1650	-1100		.20	2.30	3.05		--------	.6
1800	-1200		.18	2.30	2.50		--------	.6
2400	-1600	0.060	0.19×10^{-3}	2.80	2.87	0.75	--------	0.6
3000	-2000	↓	.21	2.25	2.85	↓	4.9×10^{-6}	↓
3600	-2400		.22	2.30	3.00		--------	
4200	-2800		.23	2.40	3.00		7.6	

[a]Electrical breakdown.

TABLE II. - Continued. INDIVIDUAL DATA POINTS

[Anode-cathode discharge voltage, -50 v; see table I for magnetic field strength and inlet flow.]

(f) Run 6

Anode total voltage and net ion acceleration voltage, V_I, v	Acceleration voltage, V_A, v	Beam current, J_B, amp	Acceleration impingement current, J_A, amp	Anode current, J_I, amp	Filament emission current, J_E, amp	Propellant utilization efficiency, η_u	Tank pressure, mm Hg	Net- to total-acceleration voltage ratio, R
1000	-250	0.063	10.2×10^{-3}	1.00	0.70	0.14	3.6×10^{-6}	0.8
1200	-300	↓	2.70	.90	----	↓	3.6	↓
1500	-375		1.86	.90	----		3.65	
2000	-500		1.97	.70	.40		3.7	
2500	-625		2.27	.60	.40		3.9	
[a]4000	[a] 1000	[a]0.063	[a]2.22×10^{-3}	[a]0.45	[a]0.30	[a]0.14	[a]4.3×10^{-6}	[a]0.8
900	-600	.063	4.86	.95	----	.14	--------	.6
1000	-666	↓	2.51	.95	.65	↓	--------	↓
1200	-800		2.08	.90	.60		3.5	
1800	-1200		2.62	.70	.50		3.7	
2400	-1600	0.063	3.35×10^{-3}	0.55	0.40	0.14	3.85×10^{-6}	0.6
3000	-2000	.063	5.40	.50	.35	.14	4.05	.6
[a]3500	[a]-2200	[a].063	(a)	(a)	(a)	[a].14	(a)	[a].61
600	-900	.063	6.93	1.00	.80	.14	3.4	.4
700	-1050	.063	2.31	.95	.65	.14	3.4	.4
800	-1200	0.063	2.61×10^{-3}	0.90	0.60	0.14	3.4×10^{-6}	0.4
1200	-1800	.063	3.35	.70	.45	.14	3.5	.4
1600	-2400	.063	3.58	.60	.40	.14	3.6	.4
[a]2000	[a]-3000	[a].063	[a]5.95	[a].55	[a].40	[a].14	[a]3.7	[a].4
2000	-500	.125	8.86	2.20	1.60	.28	3.8	.8
2200	-550	0.125	4.32×10^{-3}	2.10	----	0.28	3.7×10^{-6}	0.8
2300	-575	↓	2.65	1.95	1.40	↓	3.7	↓
2500	-625		3.00	2.00	1.50		3.8	
3000	-750		3.08	1.85	1.30		4.3	
3500	-875		3.19	1.70	1.20		4.6	
[a]3800	[a]-875	[a]0.125	(a)	(a)	(a)	[a]0.28	(a)	[a]0.81
1500	-1000	.125	5.62×10^{-3}	----	----	.28	3.4×10^{-6}	.6
1650	-1100	↓	2.94	2.00	----	↓	3.4	↓
1800	-1200		2.96	1.95	1.40		3.5	
2400	-1600		3.12	1.75	1.20		3.6	
[a]3000	[a]-2000	[a]0.125	[a]3.35×10^{-3}	[a]1.60	[a]1.10	[a]0.28	[a]3.9×10^{-6}	[a]0.6
1100	-1650	.125	9.20	1.90	1.40	.28	3.5	.4
1200	-1800	↓	4.97	1.90	1.40	↓	3.5	↓
1300	-1950		4.00	1.80	1.40		3.5	
1600	-2400		3.73	1.70	----		3.4	
2000	-3000	0.125	3.68×10^{-3}	1.50	1.00	0.28	3.6×10^{-6}	0.4
2500	-625	.187	9.72	3.30	2.40	.42	3.4	.8
2700	-650	↓	6.92	3.10	2.30	↓	3.5	↓
3000	-750		4.33	3.10	2.40		4.1	
4000	-1000		4.33	2.70	2.00		4.0	
[a]4500	[a]-1125	[a]0.125	(a)	(a)	(a)	[a]0.42	(a)	[a]0.8
1650	-1100	.125	14.5×10^{-3}	3.40	----	.42	3.3×10^{-6}	.6
1800	-1200	↓	5.85	3.30	2.50	↓	3.3	↓
1950	-1300		3.78	3.30	2.50		3.5	
2400	-1600		3.90	2.90	2.20		3.3	
3000	-2000	0.125	4.65×10^{-3}	2.60	1.90	0.42	3.6×10^{-6}	0.6
[a]3200	2100	[a].125	(a)	(a)	(a)	[a].42	(a)	[a].6
2500	-625	.250	15.7	4.80	3.70	.56	3.6	.8
2700	-675	.250	5.40	4.70	----	.56	3.9	.8
2800	-700	.250	3.90	4.60	3.50	.56	3.9	.8
3000	-750	0.250	4.65×10^{-3}	4.40	3.50	0.56	4.0×10^{-6}	0.8
3500	-875	.250	4.43	4.20	----	.56	4.3	.8
[a]4000	[a]-1000	[a].250	[a]5.40	[a]4.00	[a]2.90	[a].56	[a]4.35	[a].8
1800	-1200	.250	22.7	4.70	3.80	.56	4.0	.6
2000	-1330	.250	9.20	4.70	3.70	.56	4.1	.6
2400	-1600	0.250	5.85×10^{-3}	4.30	3.50	0.56	4.1×10^{-6}	0.6
[a]3000	[a]-2000	[a].250	[a]5.30	[a]4.00	[a]3.10	[a].56	[a]4.1	[a].6

[a]Electrical breakdown.

TABLE II. - Continued. INDIVIDUAL DATA POINTS

[Anode-cathode discharge voltage, -50 v; see table I for magnetic field strength and inlet flow.]

(g) Run 7

Anode total voltage and net ion acceleration voltage, V_I, v	Acceleration voltage, V_A, v	Beam current, J_B, amp	Acceleration impingement current, J_A, amp	Anode current, J_I, amp	Filament emission current, J_E, amp	Propellant utilization efficiency, η_u	Tank pressure, mm Hg	Net- to total-acceleration voltage ratio, R
600	-150	0.030	6.18×10^{-3}	1.00	0.80	0.17	2.0×10^{-6}	0.8
800	-200	↓	.14	.80	.65	↓	1.8	↓
1000	-250	↓	.15	.80	.60	↓	1.95	↓
2000	-500	↓	.16	.60	.45	↓	2.1	↓
4000	-1000	↓	.25	.50	.40	↓	2.2	↓
800	-200	0.050	2.18×10^{-3}	1.75	1.45	0.28	2.1×10^{-6}	0.8
900	-225	↓	.32	1.60	1.30	↓	2.1	↓
1000	-250	↓	.20	1.50	1.20	↓	2.0	↓
2000	-500	↓	.23	1.10	.90	↓	2.2	↓
4000	-1000	↓	.32	.90	.70	↓	2.6	↓
6000	-1500	0.050	0.44×10^{-3}	0.70	0.60	0.28	3.1×10^{-6}	0.8
1000	-250	.075	1.71	2.80	2.50	.43	2.3	↓
1200	-300	↓	.35	2.60	2.30	↓	2.15	↓
1400	-350	↓	.26	2.40	2.10	↓	2.0	↓
2000	-500	↓	.28	2.00	1.70	↓	2.15	↓
4000	-1000	0.075	0.38×10^{-3}	1.50	1.25	0.43	2.9×10^{-6}	0.8
5000	-1250	.075	.42	1.40	1.15	.43	3.15	↓
1400	-350	.100	1.11	4.15	4.20	.57	3.0	↓
1600	-400	.100	.34	3.80	3.70	.57	2.6	↓
2000	-500	.100	.32	3.35	3.20	.57	2.7	↓
3000	-750	0.100	0.35×10^{-3}	2.80	2.60	0.57	3.05×10^{-6}	0.8
4000	-1000	↓	.38	2.45	2.25	↓	3.5	.8
1200	-800	↓	2.60	3.90	3.85	↓	3.2	.6
1350	-900	↓	.36	3.60	3.55	↓	2.5	.6
1800	-1200	↓	.38	3.15	3.00	↓	2.6	.6
2700	-1800	0.100	0.44×10^{-3}	2.60	2.40	0.57	2.9×10^{-6}	0.6
3600	-2400	↓	.53	2.35	2.10	↓	3.4	.6
4500	-3000	↓	.63	2.02	1.80	↓	4.2	.6
1100	-1650	↓	1.19	3.30	3.20	↓	3.4	.4
1200	-1800	↓	.47	3.10	2.90	↓	3.5	.4
1400	-2100	0.100	0.44×10^{-3}	2.80	2.60	0.57	3.8×10^{-6}	0.4
2000	-3000	.100	.54	2.40	2.15	.57	4.3	.4
2000	-500	.110	.33	4.14	4.14	.63	2.8	.8
3000	-750	.115	.38	4.10	4.12	.66	3.2	.8
4000	-1000	.120	.42	4.05	4.10	.68	3.8	.8
5000	-1250	0.125	0.61×10^{-3}	4.05	4.12	0.71	4.8×10^{-6}	0.8
6000	-1500	.130	.62	4.05	4.08	.74	6.7	.8
[a]6400	[a]-1600	[a].135	(a)	(a)	(a)	[a].77	(a)	[a].8

[a]Electrical breakdown.

TABLE II. - Continued. INDIVIDUAL DATA POINTS

[Anode-cathode discharge voltage, -50 v; see table I for magnetic field strength and inlet flow.]

(d) Run 4

Anode total voltage and net ion acceleration voltage, V_T, v	Acceleration voltage, V_A, v	Beam current, J_B, amp	Acceleration impingement current, J_A, amp	Anode current, J_I, amp	Filament emission current, J_E, amp	Propellant utilization efficiency, η_u	Tank pressure, mm Hg	Net- to total-acceleration voltage ratio, R	Anode total voltage and net ion acceleration voltage, V_I, v	Acceleration voltage, V_A, v	Beam current, J_B, amp	Acceleration impingement current, J_A, amp	Anode current J_I, amp	Filament emission current, J_E, amp	Propellant utilization efficiency, η_u	Tank pressure, mm Hg	Net- to total-acceleration voltage ratio, R
1300	-150	0.031	2.27×10^{-3}	0.65	0.55	0.19	1.4×10^{-6}	[b]0.90	3000	-355	0.093	0.42×10^{-3}	1.80	1.60	0.56	2.4×10^{-6}	[b]0.90
1500	-155	↓	.67	.55	.45	↓	1.4	b.90	4000	-490	↓	.38	1.60	1.40	↓	2.7	b.89
2000	-240		.22	.50	.30		1.3	b.89	5000	-640		.40	1.40	1.30		2.6	b.89
3000	-300		.23	.40	.30		1.3	b.91	6000	-800		.45	1.30	1.11		2.6	b.88
4500	-500	↓	.31	.30	.20	↓	1.6	b.90	[a]7000	[a]-900	a.093	(a)	(a)	(a)	a.56	(a)	ab.89
6000	-375	0.031	0.24×10^{-3}	0.30	0.20	0.19	1.8×10^{-6}	[b]0.94	2000	-500	0.093	8.65×10^{-3}	2.10	1.90	0.56	--------	0.8
7000	-495	↓	.25	.30	.20	↓	2.0	b.93	2200	-550	↓	3.24	2.10	1.90	↓	2.2×10^{-6}	↓
1000	-250		6.05	.70	.60		1.3	.8	2300	-575		.86	2.00	1.80		2.0	
1300	-325		.54	.55	.45		1.3	.8	2500	-625		.42	1.90	1.70		2.2	
1500	-375	↓	.24	.50	.40	↓	1.3	.8	3000	-750	↓	.40	1.80	1.60	↓	2.4	↓
2000	-500	0.031	0.25×10^{-3}	0.40	0.35	0.19	1.3×10^{-6}	0.8	4000	-1000	0.093	0.42×10^{-3}	1.50	1.40	0.56	2.6×10^{-6}	0.8
3000	-750		.25	.35	.30		1.5		5000	-1250	.093	.54	1.40	1.20	.56	2.5	.8
4000	-1000		.28	----	----		1.7		[a]5500	[a]-1375	a.093	.62	a1.30	a1.15	.56	a2.6	a.8
5000	-1250		.28	----	----		1.75		1650	-1100	.093	4.32	2.00	1.80	.56	1.9	.6
6000	-1500	↓	.37	.30	.20	↓	1.85	↓	1800	-1200	.093	1.21	2.00	1.80	.56	1.9	.6
6500	-1625	0.031	0.33×10^{-3}	0.20	0.17	0.19	2.0×10^{-6}	0.8	1950	-1300	0.093	0.54×10^{-3}	1.80	1.60	0.56	2.1×10^{-6}	0.6
6700	-1670	[a].031	(a)	(a)	(a)	a.19	(a)	a.8	2700	-1800	.093	.50	1.60	1.40	.56	2.2	.6
750	-500	.031	6.27	.70	.60	.19	1.25	.6	3900	-2600	.093	.64	1.30	1.20	.56	2.7	.6
900	-600	.031	1.44	.60	.50	.19	1.3	.6	[a]4500	[a]-3000	a.093	a.66	a1.20	a1.10	a.56	a2.9	a.6
1050	-700	.031	.36	.50	.40	.19	1.3	.6	1100	-1650	.093	5.63	2.00	1.80	.56	1.9	.4
1200	-800	0.031	0.30×10^{-3}	0.50	0.40	0.19	1.3×10^{-6}	0.6	1200	-1800	0.093	2.38×10^{-3}	2.00	1.80	0.56	2.0×10^{-6}	0.4
1500	-1000	↓	.31	.40	.30	↓	1.35	↓	1300	-1950	↓	.56	1.80	1.70	.56	2.0	.4
1800	-1200		.32	.40	.30		1.4		1600	-2400		.55	1.70	1.60	.56	2.0	.4
2700	-1800		.35	.35	.25		1.5		2000	-3000		.56	1.50	1.30	.56	2.2	.4
3600	-2400	↓	.36	.30	.20	↓	1.6	↓	3500	-560	.125	1.43	4.00	4.20	.76	3.1	b.86
4500	-3000	0.031	0.43×10^{-3}	0.30	0.20	0.19	1.8×10^{-6}	0.6	3750	-630	0.125	0.58×10^{-3}	4.10	4.30	0.76	3.1×10^{-6}	[b]0.86
600	-900	↓	2.36	.60	.50	↓	1.25	.4	4000	-590	.125	.33	----	----	.76	3.2	b.87
700	-1050		.57	.55	.45		1.25	.4	5000	-720	.125	.35	2.90	2.90	.76	3.1	b.87
800	-1200		.33	.50	.40		1.25	.4	[a]5500	[a]-720	a.125	(a)	(a)	(a)	a.76	(a)	a.88
1400	-2100	↓	.36	.40	.30	↓	1.35	.4	3000	-750	.125	4.65	3.50	3.60	.76	2.9	.8
2000	-3000	0.031	0.39×10^{-3}	0.30	0.20	0.19	1.5×10^{-6}	0.4	3200	-800	0.125	0.92×10^{-3}	3.30	3.40	0.76	2.9×10^{-6}	0.8
2000	-250	.063	.29	1.30	1.20	.38	1.7	b.89	3300	-825	↓	.73	3.30	3.40	↓	3.0	↓
2250	-360	.063	.33	1.20	1.00	.38	1.7	b.86	3500	-1250		.44	3.10	3.10		3.1	
3000	-350	.063	.30	1.00	.85	.38	1.7	b.90	4000	-1000		.40	2.90	2.90		3.2	
4000	-300	.063	.34	.90	.80	.38	2.05	b.93	4500	-1125	↓	.45	2.80	2.80	↓	3.3	↓
5000	-400	0.063	0.37×10^{-3}	0.80	0.70	0.38	2.5×10^{-6}	[b]0.92	[a]4800	[a] 1125	[a]0.125	(a)	(a)	(a)	[a]0.76	3.3×10^{-6}	0.81
6000	-660	.063	.33	.75	.60	.38	2.2	b.91	2100	-1400	.125	4.85×10^{-3}	3.60	3.70	.76	2.7	.6
[a]7000	[a]-800	[a].063	a.35	a.75	a.60	a.38	[a]2.6	ab.90	2250	-1500	↓	2.30	3.50	3.60	↓	2.8	↓
2000	-500	.063	2.03	1.30	1.20	.38	2.2	.8	2400	-1600		1.10	3.40	3.40		2.8	
2100	-525	.063	.53	1.20	1.10	.38	2.0	.8	2550	-1700	↓	.51	3.30	3.35	↓	2.8	↓
2200	-550	0.063	0.35×10^{-3}	1.20	1.00	0.38	1.95×10^{-6}	0.8	2700	-1800	0.125	0.51×10^{-3}	3.10	3.20	0.76	2.9×10^{-6}	0.6
2500	-625	↓	.41	1.10	.90	↓	2.1		3000	-2000	.125	.54	2.80	2.90	.76	3.0	.6
3000	-750		.40	1.00	.80		2.1		3600	-2400	.125	.62	2.75	2.70	.76	3.4	.6
4000	-1000		.41	.80	.70		2.2		[a]3800	[a]-2400	a.125	(a)	(a)	(a)	a.76	(a)	a.61
5000	-1250	↓	.42	.75	.60	↓	2.8	↓	1400	-2100	.125	6.28	3.70	3.80	.76	3.1	.4
6000	-1500	0.063	0.40×10^{-3}	0.65	0.55	0.38	3.2×10^{-6}	0.8	1500	-2250	0.125	3.58×10^{-3}	3.60	3.75	0.76	3.1×10^{-6}	0.4
[a]6500	[a]-1625	[a].063	a.40	a.65	a.55	a.38	[a]3.5	a.8	1600	-2400	↓	.61	3.20	3.25	↓	3.0	↓
1200	-800	.063	9.15	1.40	1.30	.38	2.35	.6	1800	-2700		.53	3.20	3.30		2.9	
1350	-900	.063	2.46	1.35	1.20	.38	2.15	.6	2000	-3000		.55	3.10	3.15		2.9	
1500	-1000	.063	1.08	1.30	1.20	.38	2.05	.6	3250	-555	.133	2.84	4.40	4.65	.80	2.8	b.86
1650	-1100	0.063	0.41×10^{-3}	1.20	1.10	0.38	2.0×10^{-6}	0.6	3500	-600	0.133	0.83×10^{-3}	4.30	4.55	0.80	3.0×10^{-6}	[b]0.86
2100	-1400	↓	.41	1.00	----	↓	1.95		4000	-630	.133	.33	4.30	4.60	.80	--------	b.86
2700	-1800		.42	.90	----		2.1		5000	-850	.133	.35	4.20	4.60	.80	3.5	b.86
3300	-2200		.44	.80	----		2.3		3000	-750	.131	3.90	4.20	4.40	.79	--------	.8
3900	-2600	↓	.46	.80	.65	↓	2.6	↓	3200	-800	.131	1.08	4.20	4.40	.79	2.9	.8
[a]4500	[a]-3000	[a]0.063	[a]0.52×10^{-3}	[a]0.70	[a]0.60	[a]0.38	[a]2.9×10^{-6}	[a]0.6	3500	-875	0.131	0.38×10^{-3}	4.10	4.30	0.79	3.0×10^{-6}	0.8
900	-1350	.063	47.5	1.40	1.20	.38	2.2	.4	4000	-1000	.131	.36	4.20	4.40	.79	--------	.8
1000	-1500	↓	.94	1.30	1.20	↓	2.3		[a]4500	[a]-1125	a.131	.37	[a]4.20	[a]4.40	a.79	[a]3.4	a.8
1100	-1650		.44	1.20	----		2.2		2100	-1400	.133	5.85	4.30	4.40	.80	2.9	.6
1200	-1800	↓	.47	1.10	1.00	↓	2.5	↓	2400	-1600	.133	1.55	4.30	4.60	.80	2.85	.6
1600	-2400	0.063	0.45×10^{-3}	0.95	0.80	0.38	2.4×10^{-6}	0.4	2550	-1700	0.133	0.63×10^{-3}	4.40	4.60	0.80	2.9×10^{-6}	0.6
2000	-3000	.063	.50	.80	.70	.38	2.7	.4	3000	-2000	↓	.45	4.20	4.40	↓	--------	↓
2250	-340	.093	6.92	2.10	2.00	.56	2.1	b.87	3600	-2400		.49	4.20	4.40		3.4	
2500	-400	.093	1.49	2.00	1.90	.56	2.2	b.86	4050	-2700		.55	4.20	4.40		3.9	
2750	-450	.093	.42	1.90	1.70	.56	2.2	b.86	[a]4400	[a]-2700	a.133	(a)	(a)	(a)	a.80	(a)	a.62

[a]Electrical breakdown.

[b]Minimum $|V_A|$ to stop electron backstreaming.

TABLE II. - Continued. INDIVIDUAL DATA POINTS

[Anode-cathode discharge voltage, -50 v; see table I for magnetic field strength and inlet flow.]

(e) Run 5

Anode total voltage and net ion acceleration voltage, V_I, v	Acceleration voltage, V_A, v	Beam current, J_B, amp	Acceleration impingement current, J_I, amp	Anode current, J_I, amp	Filament emission current, J_E, amp	Propellant utilization efficiency, η_u	Tank pressure, mm Hg	Net- to total-acceleration voltage ratio, R
1600	-400	0.062	6.05×10^{-3}	1.00	0.80	0.19	--------	0.8
1800	-450	↓	2.16	1.00	.75	↓	3.8×10^{-6}	↓
2000	-500		1.21	.95	.70		--------	
2400	-600		1.19	.80	.60		--------	
3000	-750		1.28	.80	.60		--------	
3600	-900	0.062	1.33×10^{-3}	0.75	0.50	0.19	3.9×10^{-6}	0.8
4000	-1000	.062	1.36	.65	.45	.19	--------	↓
5000	-1250	.062	1.45	.60	.40	.19	3.9	
2600	-650	.125	10.8	2.25	1.80	.38	--------	
2800	-700	.125	4.10	2.20	1.70	.38	--------	
3000	-750	0.125	2.36×10^{-3}	2.10	1.80	0.38	--------	0.8
3600	-900	↓	1.88	1.90	1.50	↓	--------	↓
4000	-1000		1.82	1.90	1.40		--------	
4600	-1150		1.86	1.75	1.30		4.3×10^{-6}	
5600	-1400		2.00	1.65	1.25		--------	
3000	-750	0.187	17.5×10^{-3}	3.55	2.80	0.57	--------	0.8
3500	-875	↓	3.35	3.35	2.65	↓	--------	↓
3800	-950		2.07	3.35	2.60		--------	
4000	-1000		2.08	3.20	2.50		--------	
5000	-1250		2.08	2.95	2.30		4.3×10^{-6}	
6000	-1500	0.187	2.20×10^{-3}	2.65	1.95	0.57	4.1×10^{-6}	0.8
[a]8000	[a]-2000	[a].187	(a)	(a)	(a)	[a].57	(a)	[a].8
4000	-1000	.250	5.20	5.15	4.20	.77	4.4	.8
4300	-1075	.250	2.11	4.70	3.80	.77	--------	.8
4500	-1125	.250	2.08	4.95	4.00	.77	--------	.8
5000	-1250	0.250	2.07×10^{-3}	4.65	3.70	0.77	--------	0.8
6000	-1500	.250	2.15	4.10	3.25	.77	--------	.8
[a]6200	[a]-1550	[a].250	(a)	(a)	(a)	[a].77	(a)	[a].8

[a]Electrical breakdown.

TABLE II. - Continued. INDIVIDUAL DATA POINTS

[Anode-cathode discharge voltage, -50 v; see table I for magnetic field strength and inlet flow.]

(h) Run 8

Anode total voltage and net ion acceleration voltage, V_I, v	Acceleration voltage, V_A, v	Beam current, J_B, amp	Acceleration impingement current, J_A, amp	Anode current, J_I, amp	Filament emission current, J_E, amp	Propellant utilization efficiency, η_u	Tank pressure, mm Hg	Net- to total-acceleration voltage ratio, R
1000	-250	0.087	11.0×10^{-3}	1.60	1.40	0.19	2.35×10^{-6}	0.8
1200	-300	↓	2.50	1.40	1.30	↓	2.3	↓
1500	-375		.98	1.20	1.10		2.4	
2500	-625		.99	.90	.90		2.5	
3500	-875		1.02	.70	.70		2.6	
4500	-1125	0.087	1.13×10^{-3}	0.70	0.70	0.19	2.8×10^{-6}	0.8
5500	-1375	.087	1.23	.60	.60	.19	3.0	
2000	-500	.175	4.00	3.20	2.90	.38	2.15	
2200	-550	.175	1.83	2.90	2.60	.38	2.2	
2500	-625	.175	1.43	2.80	2.50	.38	2.3	↓
3500	-875	0.175	1.52×10^{-3}	2.30	2.0	0.38	2.6×10^{-6}	0.8
4500	-1125	.175	1.64	1.90	1.70	.38	2.9	.8
[a]5500	[a]-1375	[a].175	[a]1.81	[a]1.70	[a]1.50	[a].38	[a]3.1	[a].8
2700	-675	.268	5.00	5.40	4.90	.58	1.85	.8
3000	-750	.268	2.32	5.00	4.60	.58	2.4	.8
4000	-1000	0.268	2.28×10^{-3}	4.20	3.70	0.58	2.4×10^{-6}	0.8
5000	-1250	.268	2.50	3.80	3.50	.58	2.9	
6000	-1500	.268	2.70	3.50	3.10	.58	3.2	
3500	-875	.350	5.90	8.40	7.90	.75	2.1	
4000	-1000	.350	2.03	7.60	6.90	.75	2.8	↓
4500	-1125	0.350	2.08×10^{-3}	----	----	0.75	3.1×10^{-6}	0.8
5000	-1250	.350	2.20	----	----	.75	3.25	
6000	-1500	.350	2.50	6.80	5.20	.75	3.3	
4000	-1000	.410	4.90	11.8	11.3	.92	2.7	
4500	-1125	.420	2.49	11.7	11.2	.94	2.8	
5000	-1250	.425	2.13	11.6	11.5	.95	2.9	↓

[a]Electrical breakdown.

TABLE II. - Concluded. INDIVIDUAL DATA POINTS

[Anode-cathode discharge voltage, -50 v; see table I for magnetic field strength and inlet flow.]

(1) Run 9

Anode total voltage and net ion acceleration voltage, V_I, v	Acceleration voltage, V_A, v	Beam current, J_B, amp	Acceleration impingement current, J_A, amp	Anode current, J_I, amp	Filament emission current, J_E, amp	Propellant utilization efficiency, η_u	Tank pressure, mm Hg	Net- to total-acceleration voltage ratio, R
1200	-300	0.111	11.50×10^{-3}	1.90	1.50	0.11	3.2×10^{-6}	0.8
1400	-350	↓	2.90	1.50	1.30	↓	3.0	↓
2000	-500		2.30	1.30	1.00		3.0	
3000	-750		2.35	1.00	.80		3.2	
4000	-1000		2.60	.90	.70		3.5	
5000	-1250	0.111	2.80×10^{-3}	0.90	0.70	0.11	--------	0.8
2000	-500	.220	12.00	3.70	3.10	.23	3.8×10^{-6}	↓
2200	-550	↓	5.60	3.40	2.80	↓	3.4	
2500	-625		3.60	3.40	2.60		3.5	
3000	-750		3.80	3.00	2.50		3.8	
4000	-1000	0.220	4.00×10^{-3}	2.50	2.10	0.23	4.4×10^{-6}	0.8
5000	-1250	↓	4.20	2.30	1.90	↓	5.2	↓
6000	-1500		4.30	1.90	1.50		6.1	
7000	-1750		4.60	1.90	1.50		6.6	
3000	-750	.327	9.30	5.60	4.50	.34	4.5	
4000	-1000	0.327	5.20×10^{-3}	4.80	3.90	0.34	5.0×10^{-6}	0.8
5000	-1250	.327	5.40	4.20	3.30	.34	6.0	.8
[a]6000	[a]-1500	[a].327	[a]5.60	[a]3.70	[a]3.00	[a].34	[a]7.0	[a].8
3000	-750	.375	16.40	6.70	5.20	.39	5.0	.8
3500	-875	.375	7.20	6.50	5.00	.39	--------	.8
4000	-1000	0.375	5.80×10^{-3}	6.20	4.90	0.39	--------	0.8
5000	-1250	.375	6.10	5.30	4.10	.39	--------	.8
5500	-1375	.375	6.20	4.60	3.60	.39	6.1×10^{-6}	.8
[a]6000	[a]-1500	[a].375	[a]6.50	(a)	(a)	[a].39	(a)	[a].8
3500	-875	.525	16.5	10.5	8.9	.54	5.4	.8
4000	-1000	0.525	11.2×10^{-3}	9.9	8.3	0.54	6.0×10^{-6}	0.8
4500	-1125	↓	5.4	8.8	7.2	↓	5.7	↓
5000	-1250		5.5	8.5	7.1		6.0	
5500	-1375		5.7	8.3	7.1		6.4	
[a]6000	[a]-1500	[a].525	[a]5.8	[a]8.2	[a]7.0	[a].54	(a)	[a].8
5500	-1375	0.550	7.6×10^{-3}	9.4	7.4	0.57	5.8×10^{-6}	0.8
[a]6000	[a]-1500	[a].550	[a]8.1	[a]9.2	[a]7.2	[a].57	(a)	[a].8

[a]Electrical breakdown.

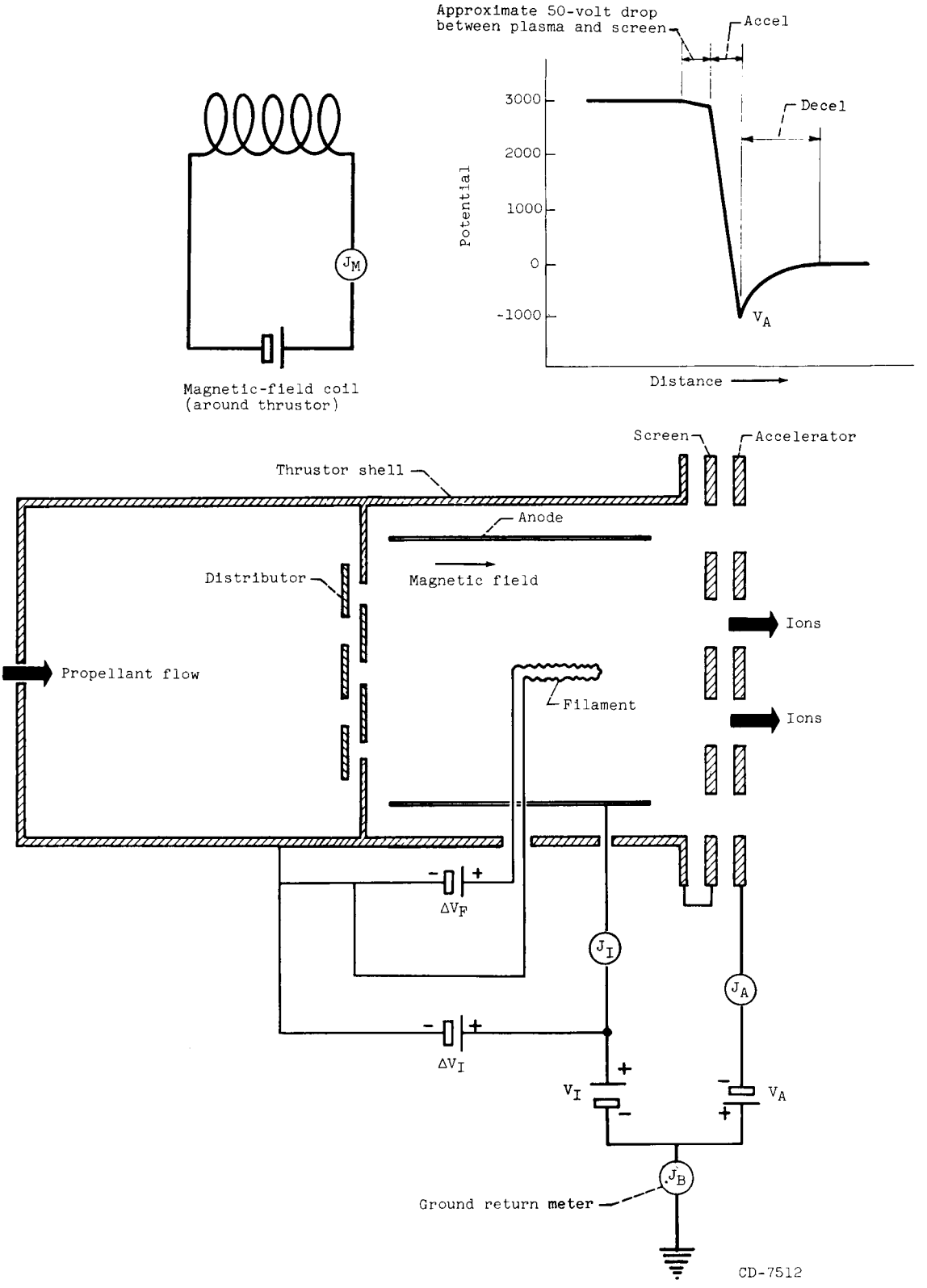

Figure 3. - Electrical diagram and potential profile of ion thrustor with an electron-bombardment ion source.

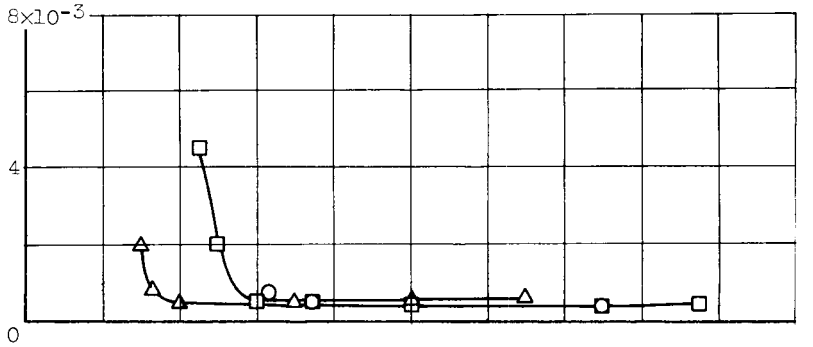

(a) 5-Centimeter-diameter thrustor. Beam current, 0.062 ampere.

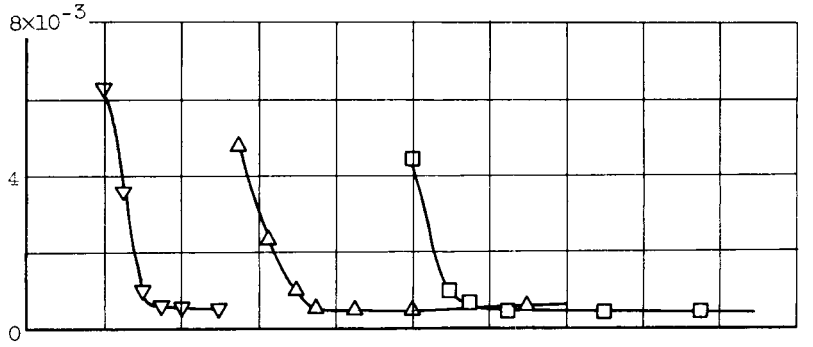

(b) 10-Centimeter-diameter thrustor. Beam current, 0.125 ampere.

Accelerator impingement current, J_A, amp

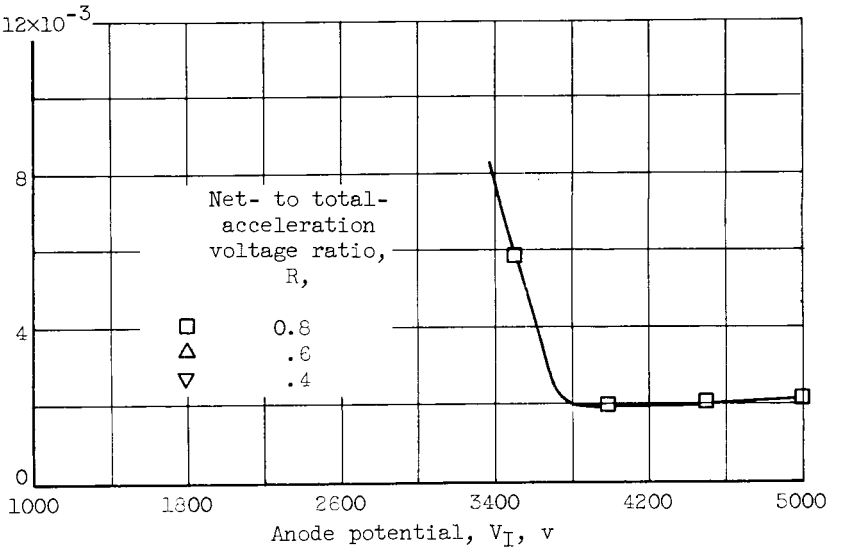

(c) 20-Centimeter-diameter thrustor. Beam current, 0.350 ampere.

Figure 4. - Typical data of accelerator impingement current as a function of anode potential for three sizes of thrustors. Propellant utilization efficiency, approximately 0.8.

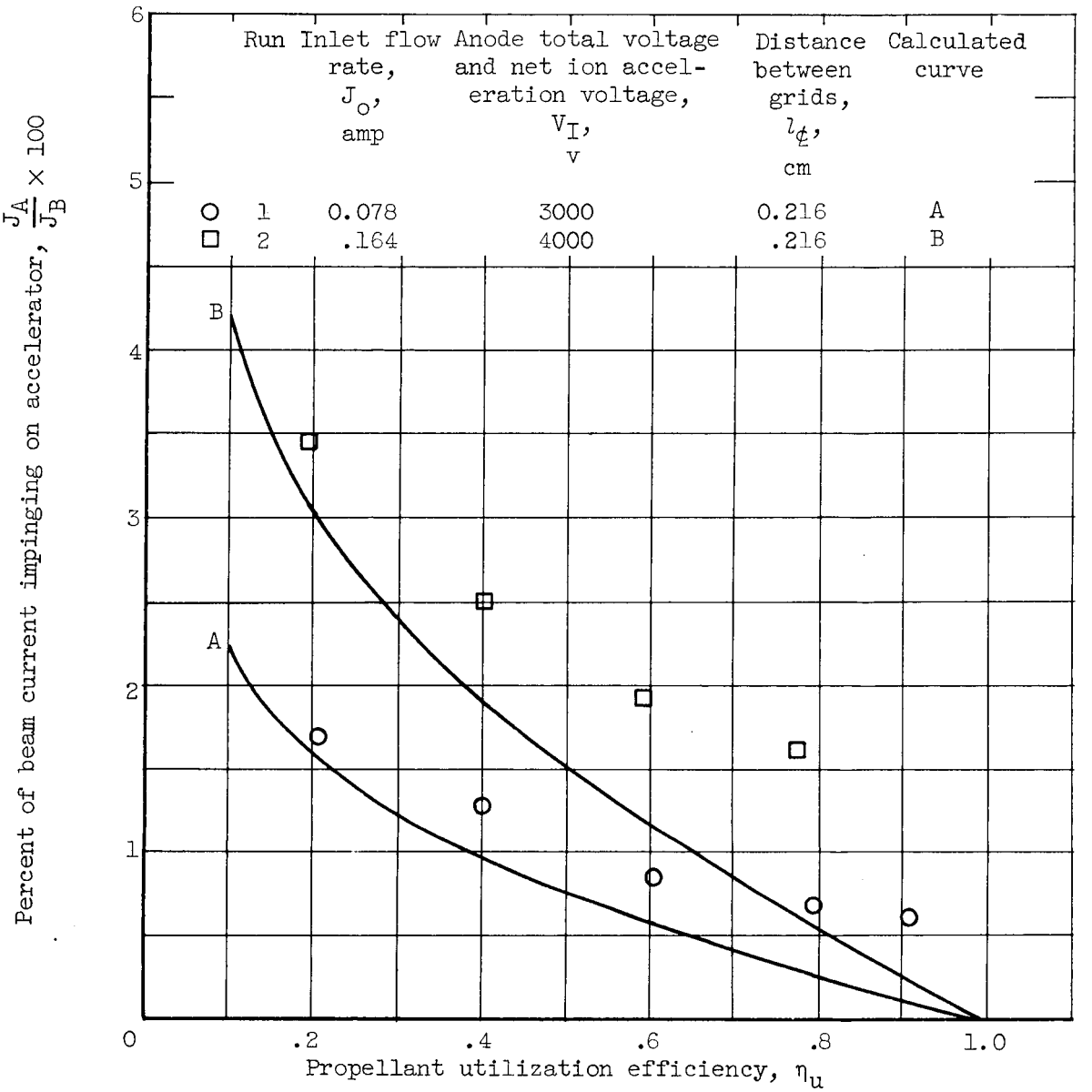

(a) 5-Centimeter-diameter thrustor. Net- to total-acceleration voltage ratio, 0.8.

Figure 5. - Percent of impingement current (measured) or charge-exchange current (calculated from eq. (B15)) as a function of propellant utilization efficiency.

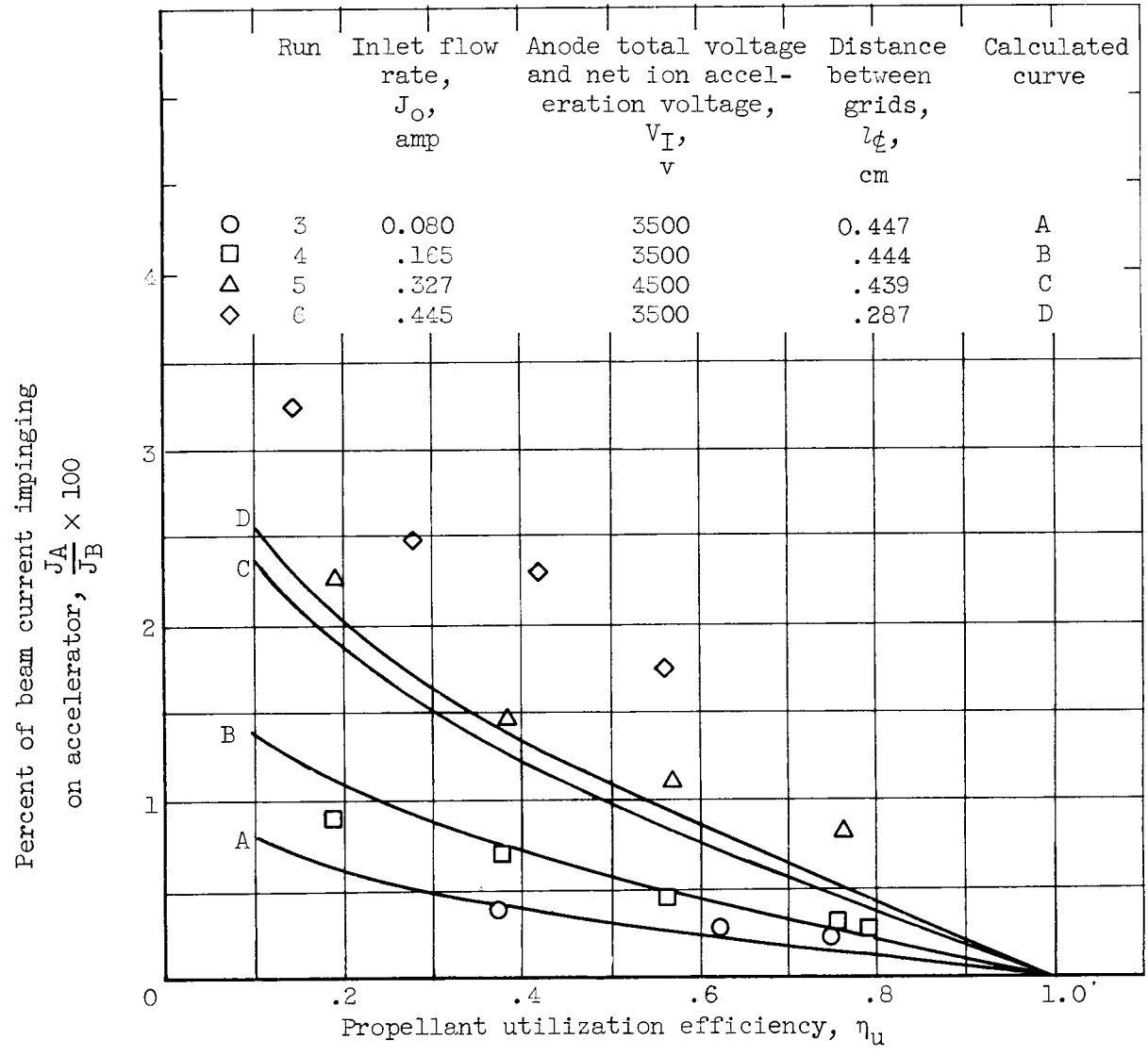

(b) 10-Centimeter-diameter thrustor. Net- to total-acceleration voltage ratio, 0.8.

Figure 5. - Continued. Percent of impingement current (measured) or charge-exchange current (calculated from eq. (B15)) as a function of propellant utilization efficiency.

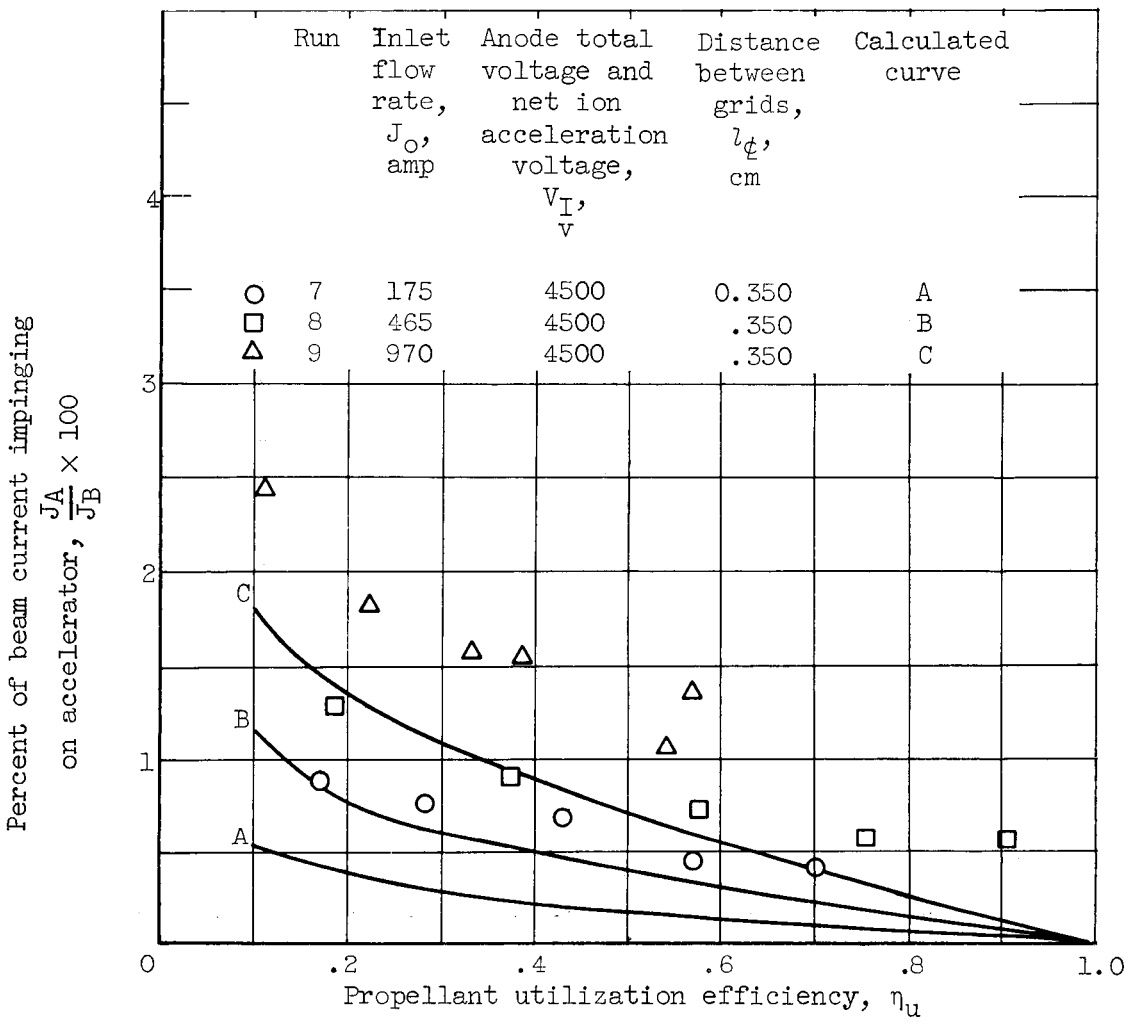

(c) 20-Centimeter-diameter thrustor. Net- to total-acceleration voltage ratio, 0.8.

Figure 5. - Continued. Percent of impingement current (measured) or charge-exchange current (calculated from eq. (B15)) as a function of propellant utilization efficiency.

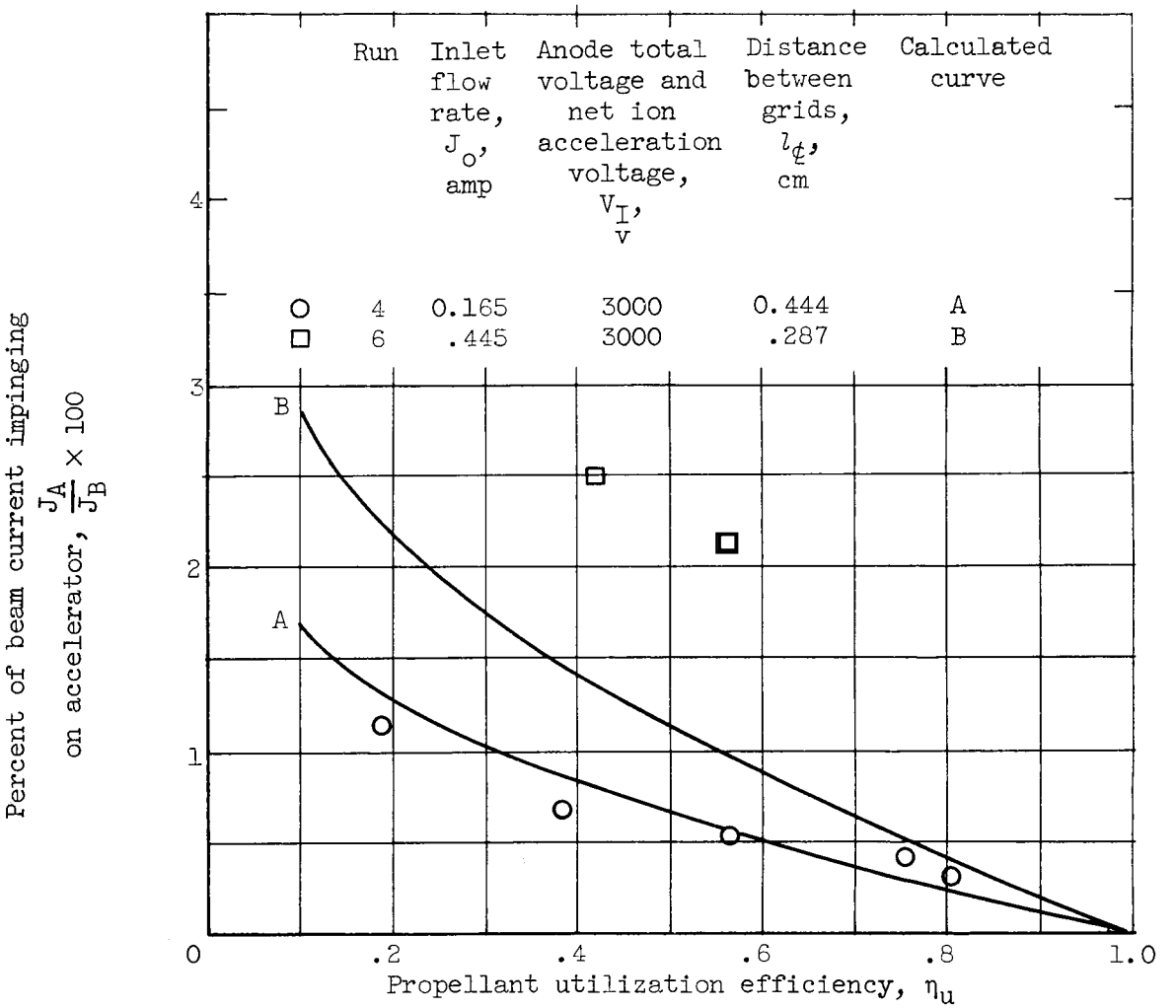

(d) 10-Centimeter-diameter thrustor. Net- to total-acceleration voltage ratio, 0.6.

Figure 5. - Continued. Percent of impingement current (measured) or charge-exchange current (calculated from eq. (B15)) as a function of propellant utilization efficiency.

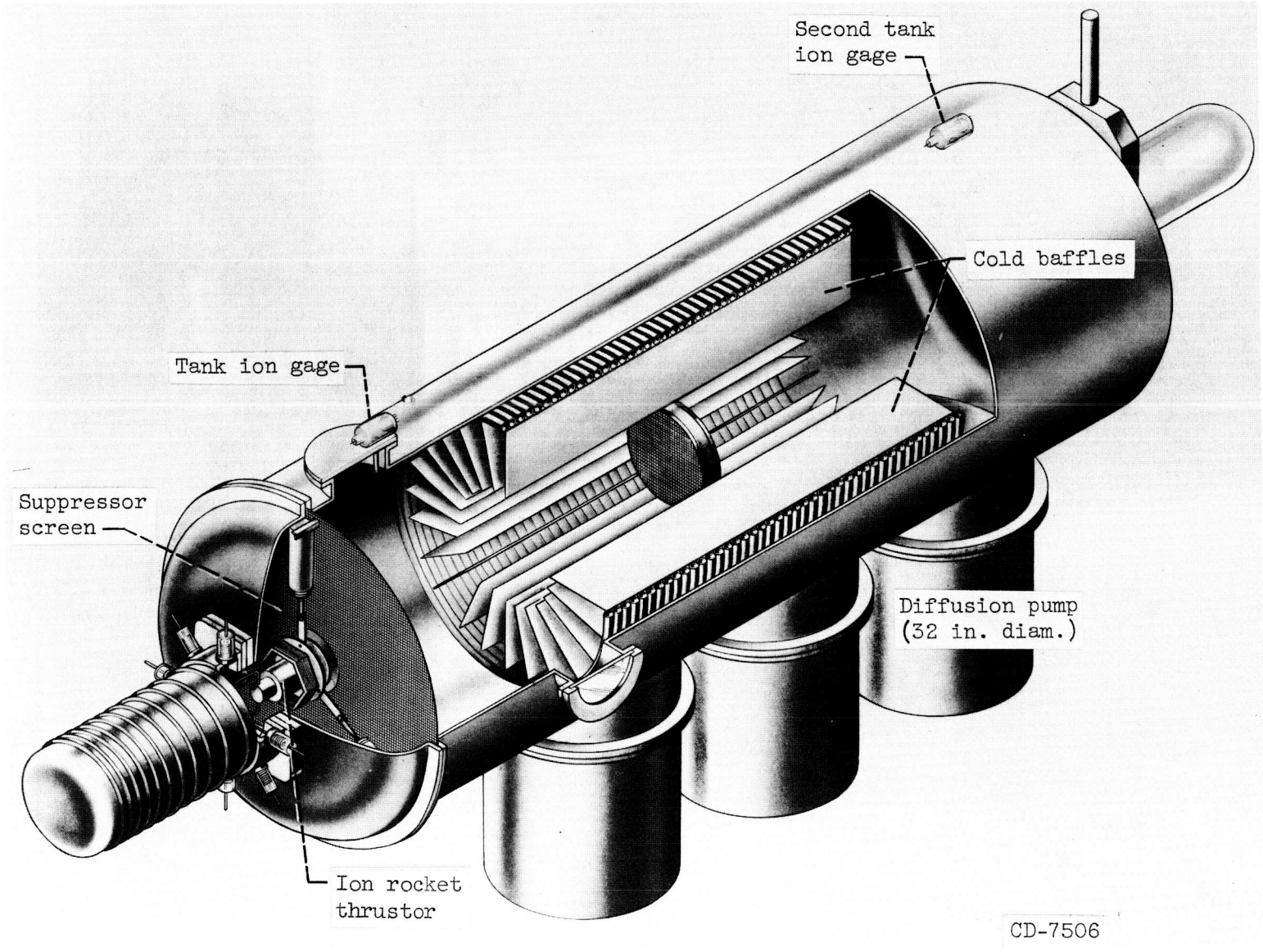

Figure 1. - Cutaway drawing of vacuum tank.

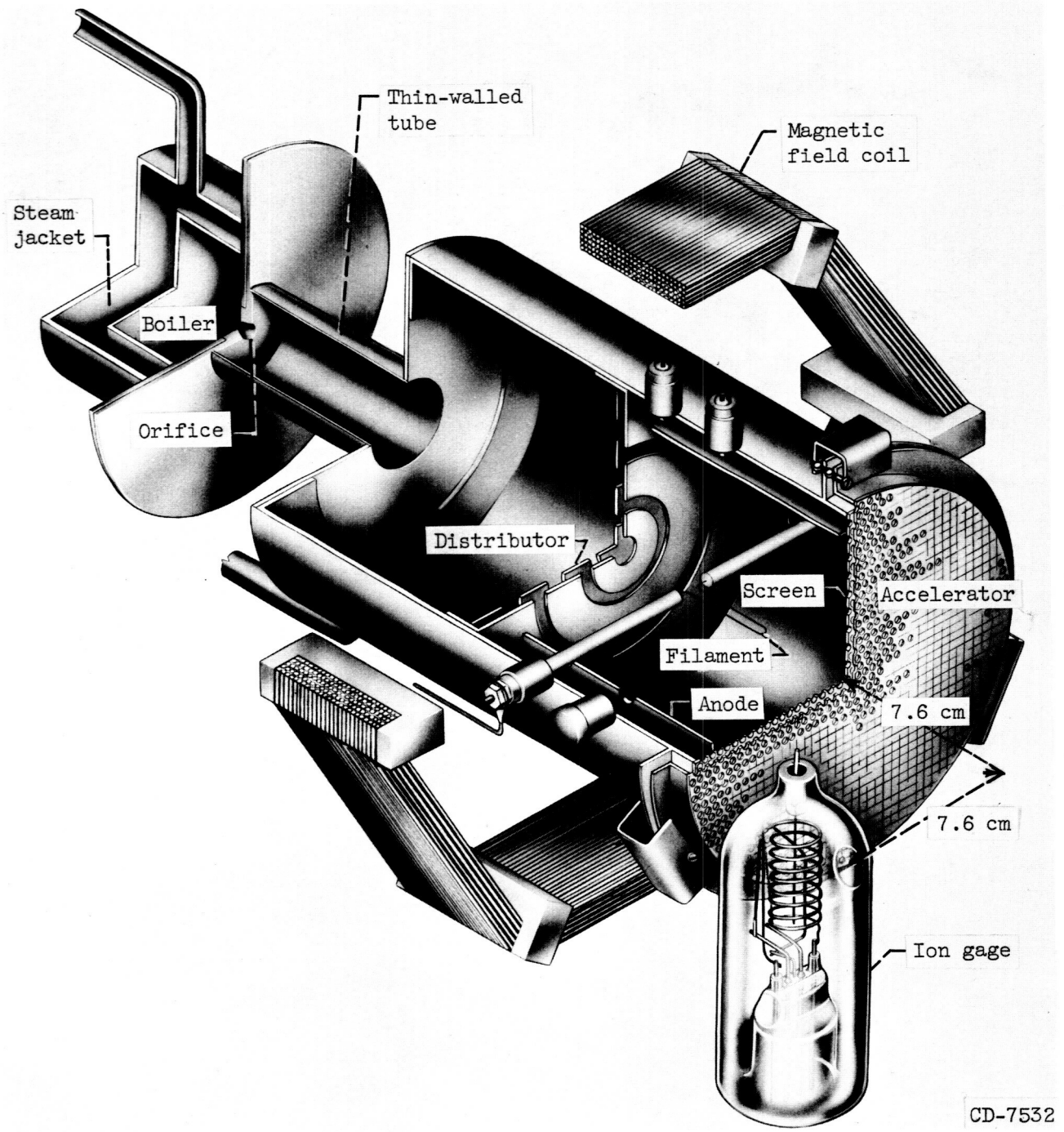

Figure 2. - Cutaway sketch of 10-centimeter-diameter electron-bombardment thrustor including the location of ionization gage, 7.6 centimeters downstream and 7.6 centimeters radially from the centerline.

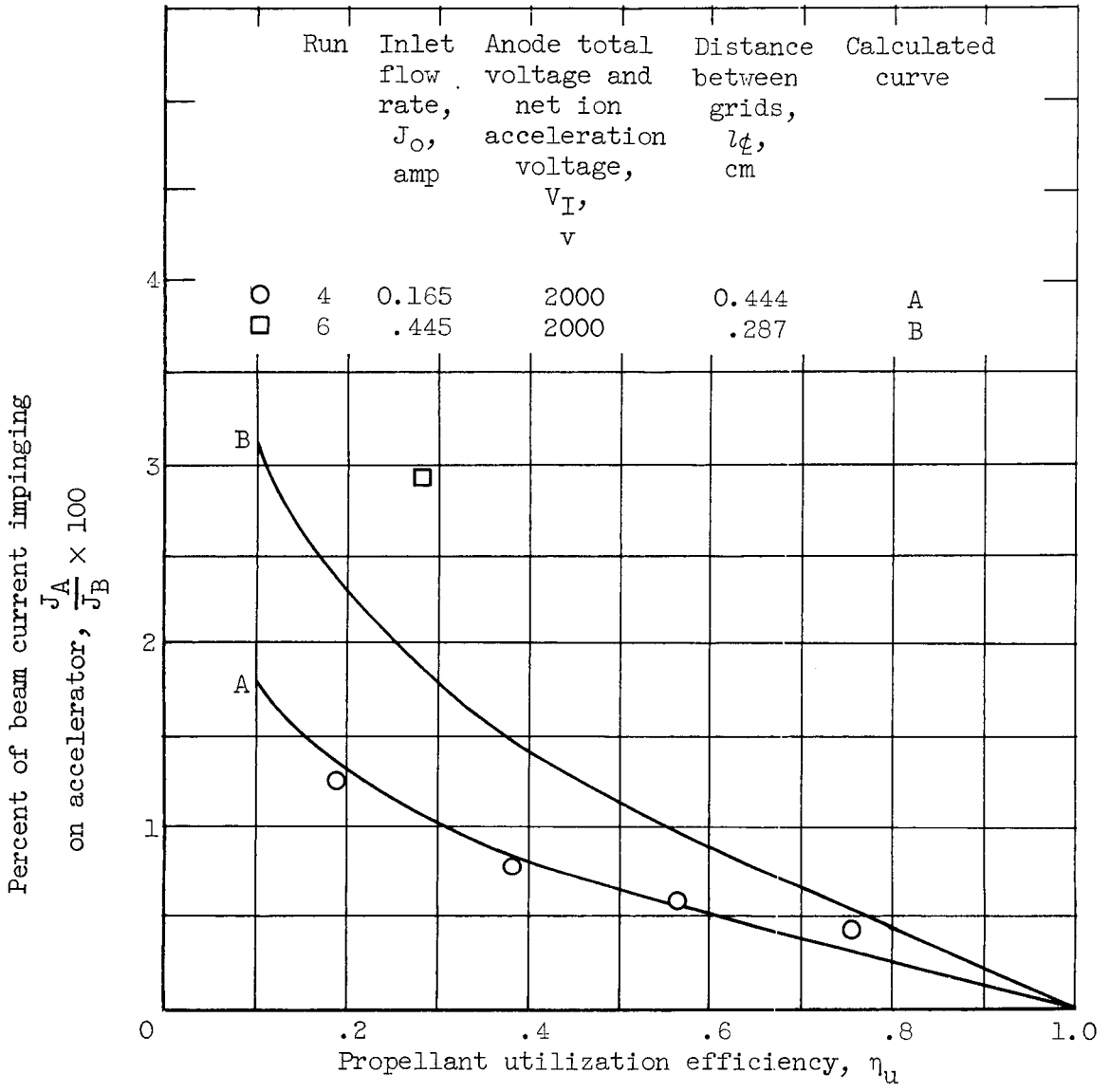

(e) 10-Centimeter-diameter thrustor. Net- to total-acceleration voltage ratio, 0.4.

Figure 5. - Concluded. Percent of impingement current (measured) or charge-exchange current (calculated from eq. (B15)) as a function of propellant utilization efficiency.

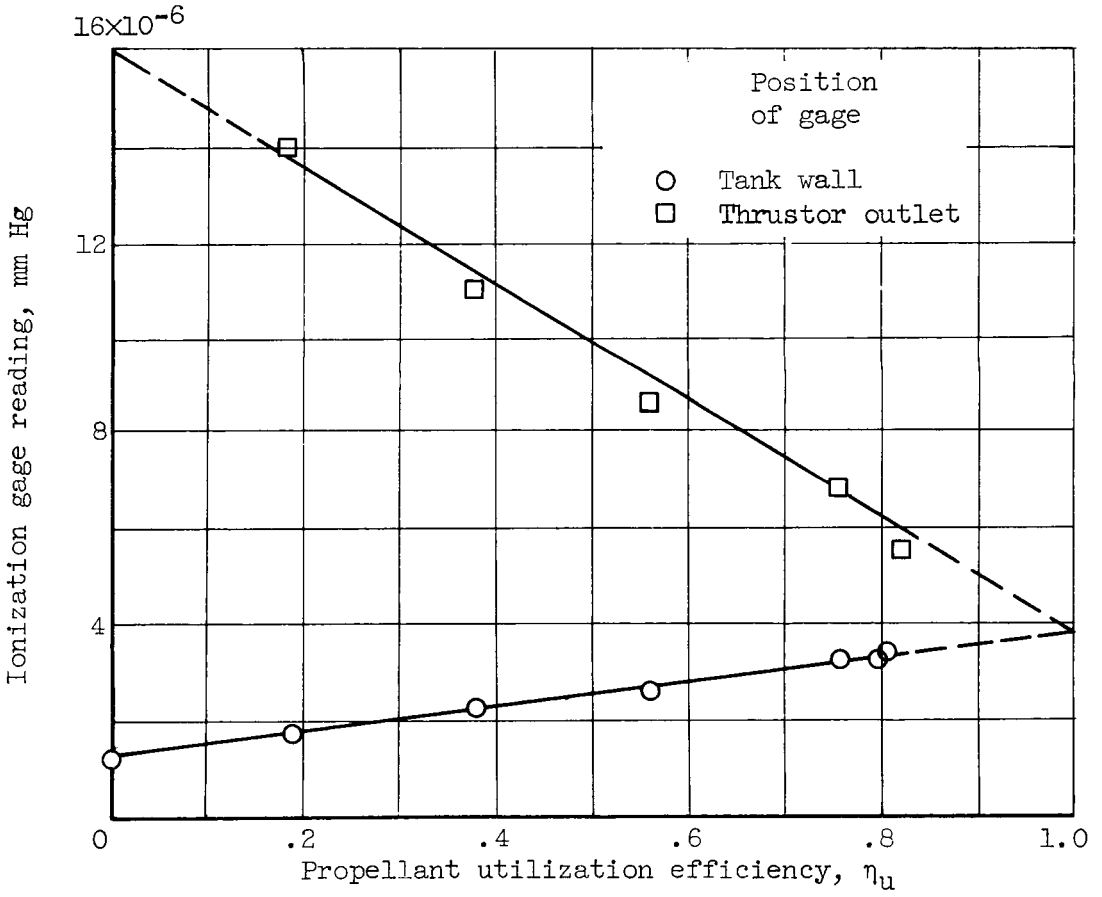

Figure 6. - Ionization gage reading as a function of propellant utilization efficiency for run 4. Anode total voltage and net ion acceleration voltage, 4000 volts; accelerator voltage, 1000 volts; inlet flow rate, 0.165 amperes; thrustor diameter, 10 centimeters. (For gage locations see fig. 1 or 2.)

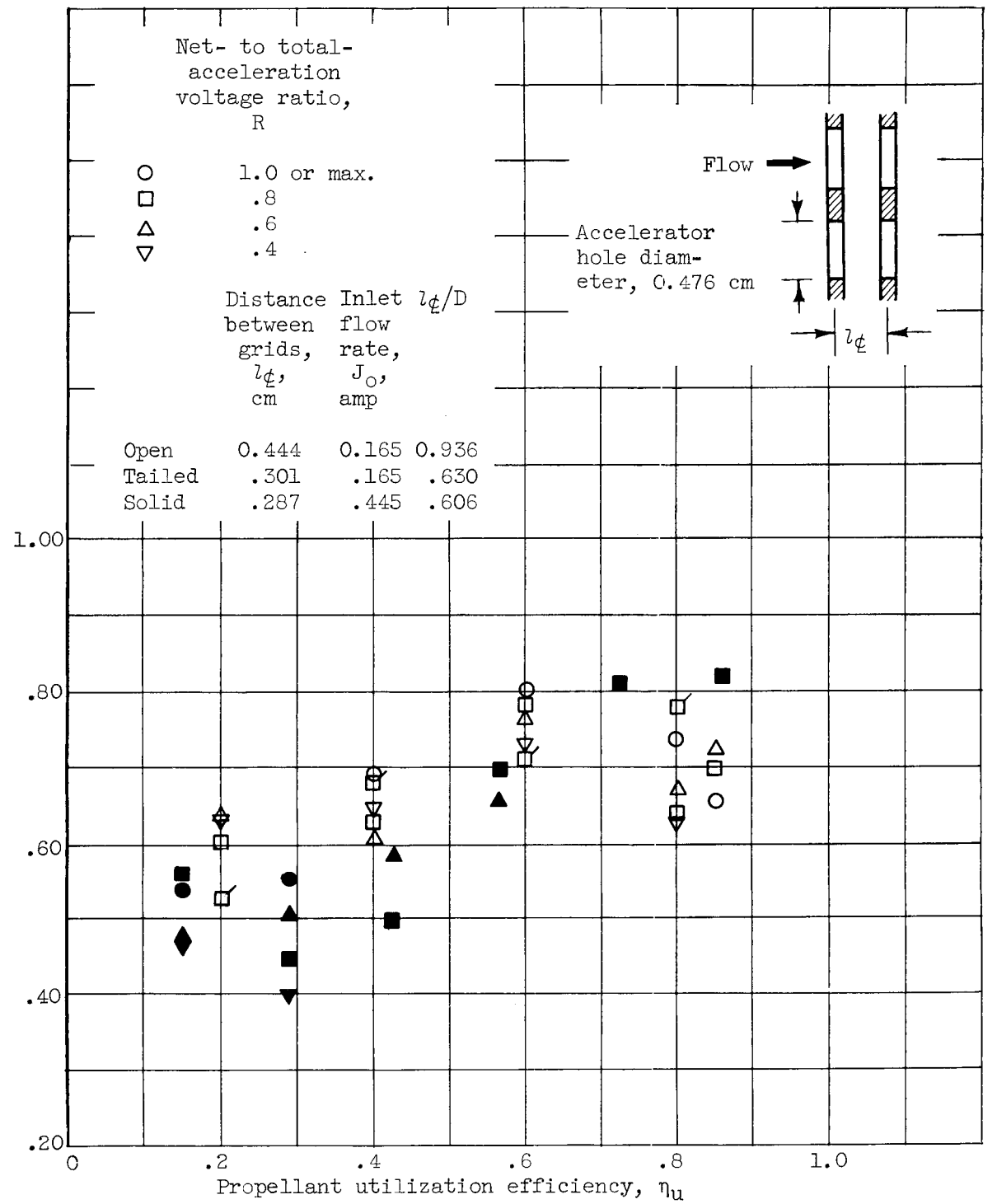

Figure 7. - Fraction of current determined by Child's law passing through screen-accelerator grids of the 10-centimeter-diameter thrustor. Child's law equation (ref. 1): $J_B = 0.386 \times 10^{-8} \frac{A_A(\Delta V)^{3/2}}{l_{\ell}^2}$.

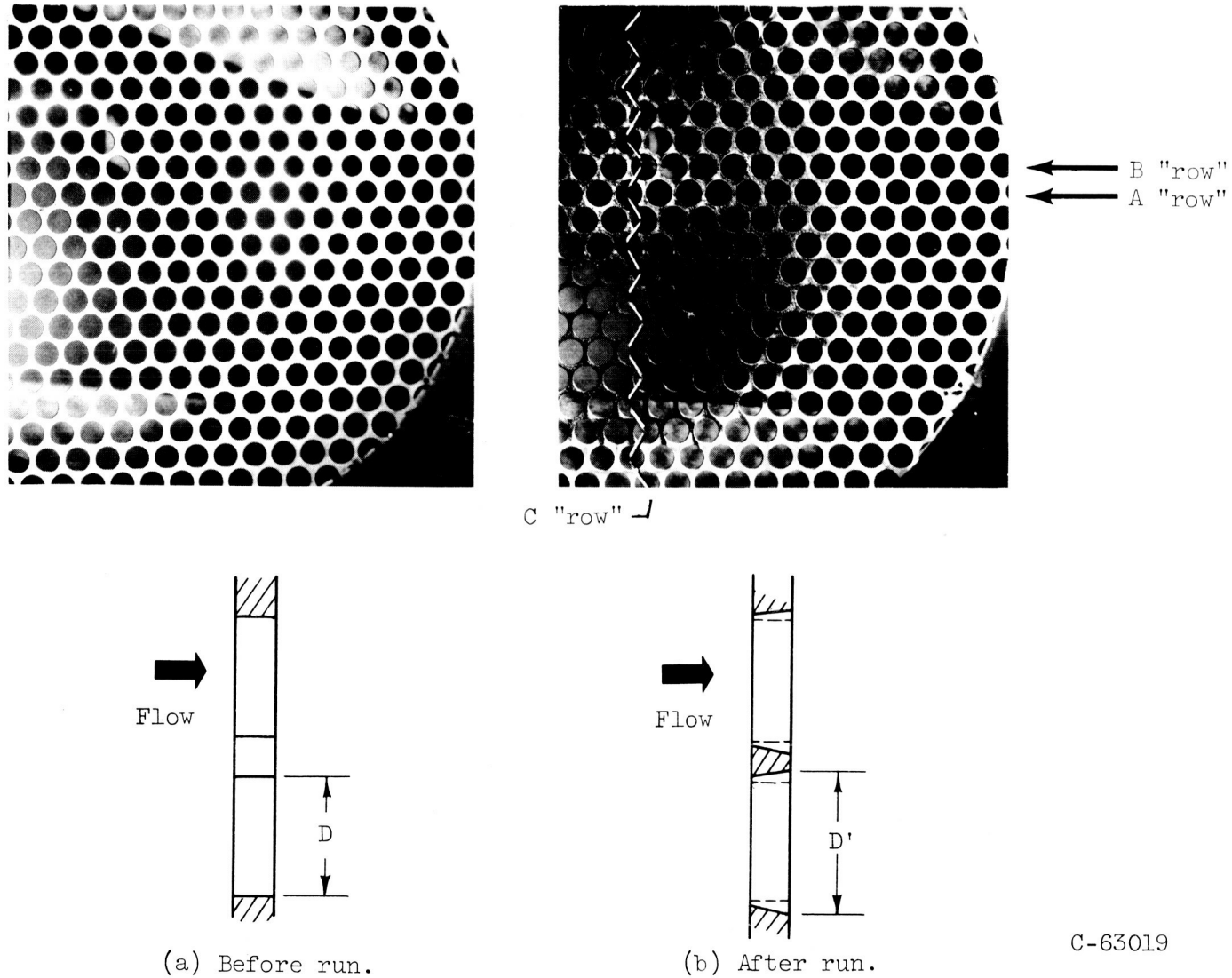

Figure 8. - Photograph and sketch of accelerator grid downstream face before and after endurance run of 150 hours (ref. 2). Thrustor diameter, 10 centimeters; beam current, 0.20 ampere; anode total voltage and net ion acceleration voltage, 2500 volts; accelerator impingement current, 4×10^{-3} ampere.

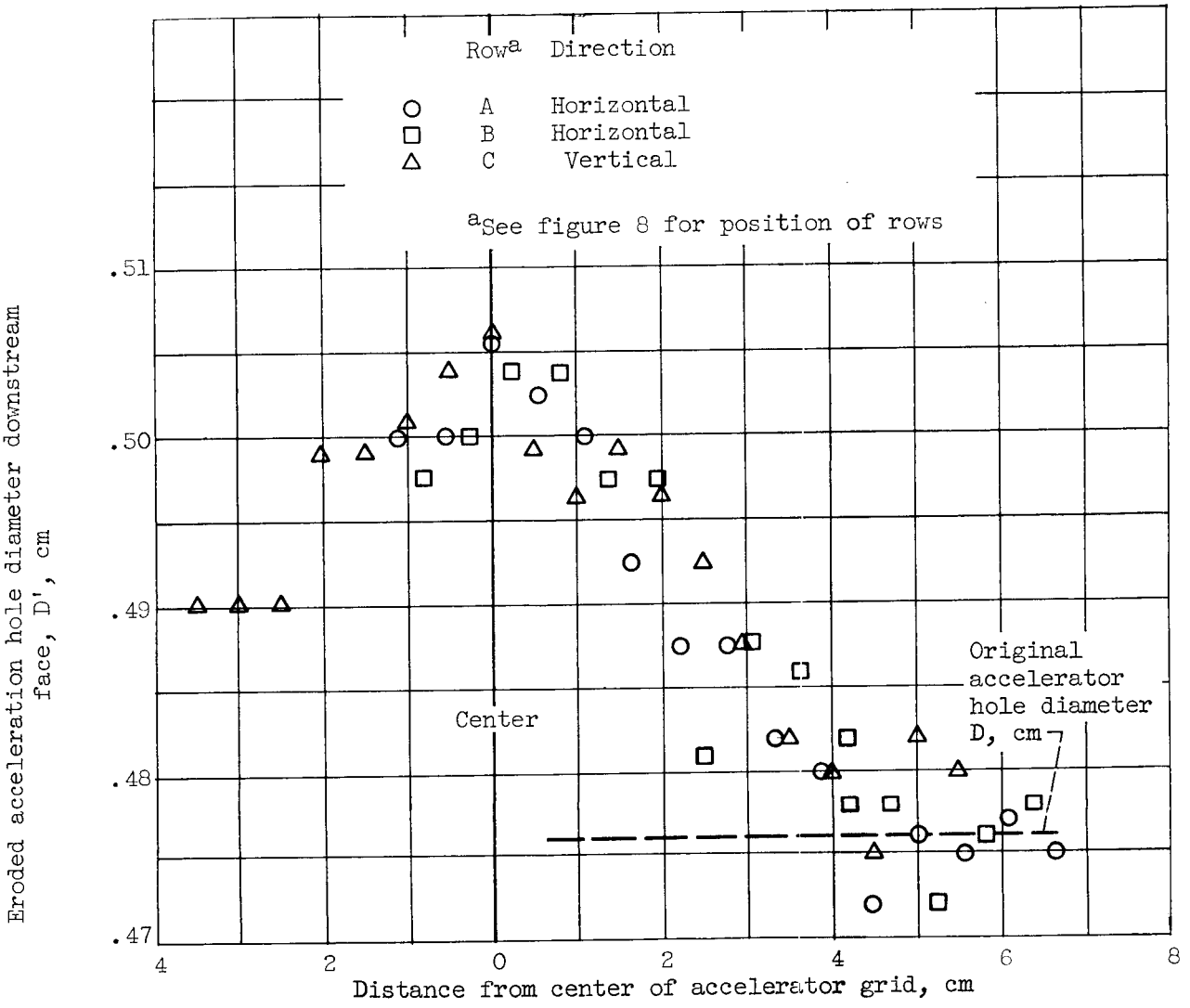

Figure 9. - Enlargement of accelerator grid hole as a function of radial distance. Measurement was made on the downstream face after 150-hour endurance run.

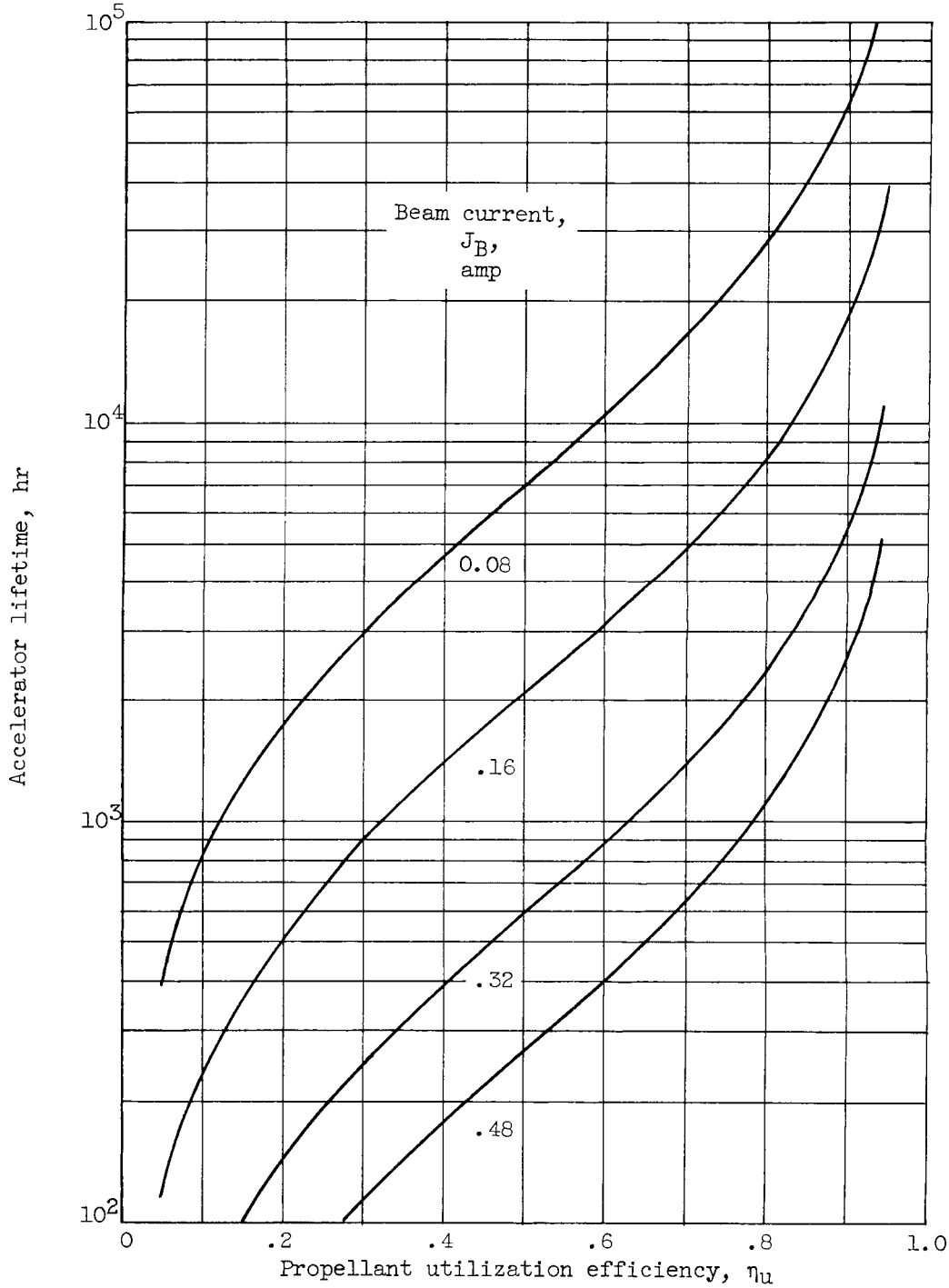

Figure 10. - Calculated lifetime of accelerator grid due to erosion from charge-exchange ions only. Thrustor diameter, 10 centimeters; anode total voltage and net ion acceleration voltage, 3000 volts; net- to total-acceleration voltage ratio, 0.8; distance between grid, 0.4 centimeter; accelerator grid, 0.475-centimeter-diameter holes in 0.127-centimeter-thick plate.

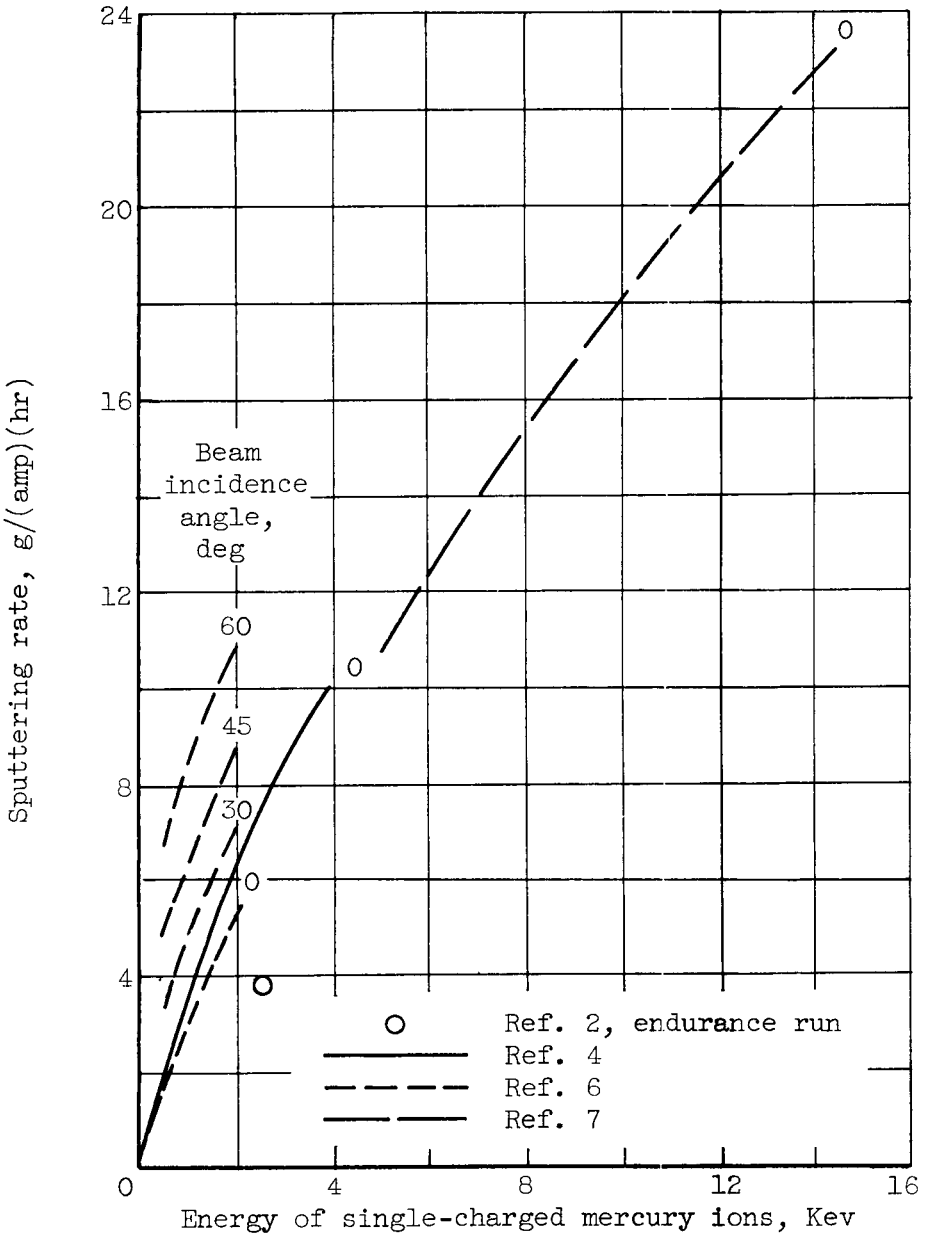

Figure 11. - Sputtering rate of molybdenum target by single-charged mercury ions.

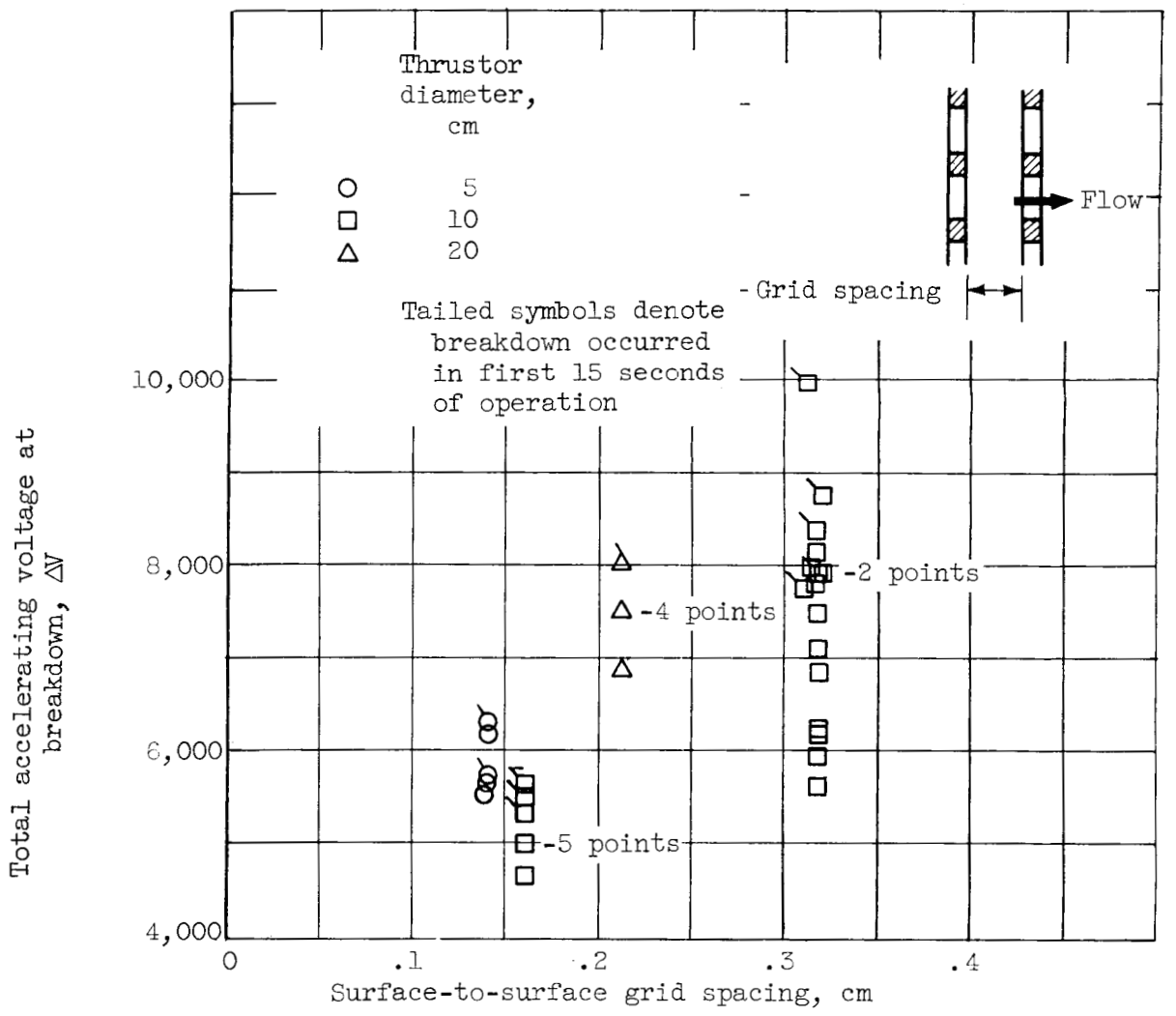

Figure 12. - Breakdown potentials of the ion thrustors while operating at beam currents of 0.03 to 0.55 ampere and net- to total-accelerating voltage ratio values of 0.4 to 0.9.